2020-02

Lawsone, lawsone ether and bilawsone for dyesensitized solar cells application

Makoye, Amosi

NM-AIST

https://doi.org/10.58694/20.500.12479/960

LAWSONE, LAWSONE ETHER AND BILAWSONE FOR DYE-SENSITIZED SOLAR CELLS APPLICATION

Amosi Makoye

A Dissertation Submitted in Partial Fulfillment of the Requirements for the Degree of Master's of Science in Materials Science and Engineering of the Nelson Mandela African Institution of Science and Technology

Arusha, Tanzania

February, 2020

ABSTRACT

Dye-sensitized solar cells (DSSCs) had turned up as a novel class of low-cost solar cells that can be fabricated easily compared to silicon solar cells. The DSSCs based on natural sensitizers are able to generate clean energy at low production cost. The modification of natural dyes facilitates the broadening of the light absorption range and improving overall DSSCs performance. In this work structural and optoelectronic properties of lawsone (L), lawsone ether (LE) and bilawsone (BL) were studied theoretically using the density functional theory (DFT) and time-dependent density functional theory methods with hybrid functional B3LYP5 and 6-311G(2d,p) basis set. The electronic spectra of the dyes molecules in a vacuum and solvents (dimethyl sulfoxide (DMSO) and dichloromethane (CH_2Cl_2)) were computed. The maximum wavelengths were found at 355-408 nm for LE and 350-448 nm for BL that indicated bands shift to visible range compared to L, 340 nm. The UV-Vis spectra of bilawsone and lawsone in dimethyl sulfoxide solution were measured experimentally. For the BL, a broad and intensive band was observed in a visible region at ~450 nm that apparently would favour sensitizing ability of the dye. The performance of DSSCs sensitized with lawsone and bilawsone were tested in outdoor conditions and I-V curves were measured. The power conversion efficiency of DSSCs sensitized with bilawsone was 1.7%, and 0.6% with lawsone. The results of the experimental measurements were in accordance with the theoretical prediction of the optoelectronic properties of the dyes. The optoelectronic properties of the LE and BL showed them as more promising candidates for DSSCs applications compared to individual lawsone dye. Therefore, the energy conversion efficiency of the cell using bilawsone dye revealed the enhancement in the cell performance.

Keywords: Lawsone isomers, Lawsone ether, Bilawsone, Dye-sensitized solar cells, UV-Vis/vibrational spectra, DFT/TD-DFT, Power conversion efficiency.

DECLARATION

I, **AMOSI MAKOYE** do hereby declare to the Senate of The Nelson Mandela African Institution of Science and Technology that this dissertation is my original work and that it has neither been submitted nor being concurrently submitted for degree award in any other institution.

Amosi Makoye

_____ _____

Name and signature of candidate **Date**

The above declaration is confirmed

Prof. Alexander Pogrebnoi

_____ _____

Name and signature of supervisor 1 **Date**

Prof. Tatiana Pogrebnaya

_____ _____

Name and signature of supervisor 2 **Date**

COPYRIGHT

CERTIFICATION

The undersigned certifies that they have read and hereby recommend for acceptance by The Nelson Mandela African Institution of Science and Technology a dissertation entitled; ***Lawsone, Lawsone Ether and Bilawsone for Dye-Sensitized Solar Cells Application,*** in partial fulfillment of the requirement for the degree of Master's of Science in Materials Science and Engineering of the Nelson Mandela African Institution of Science and Technology.

Principal supervisor

Prof. Alexander Pogrebnoi

_____ _____

Signature Date

Co-supervisor

Prof. Tatiana Pogrebnaya

_____ _____

Signature Date

ACKNOWLEDGEMENT

I wish to express my sincere gratitude to my supervisors; Prof. Alexander Pogrebnoi and Prof. Tatiana Pogrebnaya for their wisdom, advice, assistance, patience, immense knowledge and the highest level of commitment that they have shown to the completion of this dissertation. If not their close supervision, this dissertation would not have been completed. Special thanks are expressed to my sponsor; African Development Bank (AfDB) P-Z1-IA0-016 with grand No. 2100155032816 for providing financial assistance in undertaking my Master study in Materials Science and Engineering at the Nelson Mandela African Institution of Science and Technology.

Also, I would like to thank Arusha Technical Research Centre (ATRC) specifically Nicas Festo sincerely for providing Jenway spectrophotometer UK 6715 V1.42 model for the UV-Vis spectra measurements.

Moreover, I would like to expand my grateful appreciation to MESE Department staff who in one way or another provided me with moral support and encouragement; Dr. Yusufu A. C. Jande, Dr. Thomas Kivevele and Dr. Askwar Hilonga to mention few.

It would not be fair if I will not give sincere thanks to my fellow students of Masters in Materials Science and Engineering (MaSE); Mr. Plassidius Chengula, Mr. Kizito Mwilongo and PhD students in Materials Science and Engineering (MaSE); Mr. Geradius Deogratias and Mr. Rene Costa.

Finally and exceptionally, I would like to acknowledge my lovely wife, Mrs. Suzana Boniphace. Her tolerance of my spasmodic vulgar moods is a testament in itself of her firm devotion and love.

DEDICATION

This work is dedicated to my family, especially my lovely wife Suzana Boniphace, for her love in me. This also goes to my daughter Heavenlight and my son Brayden for their persistence and obedience during my long absence.

TABLE OF CONTENTS

LIST OF TABLES

LIST OF FIGURES

LIST OF ABBREVIATIONS AND SYMBOLS

ATRC	Arusha technical research centre
B3LYP5	Becke's three-parameter and lee –yang–parr functional
BL	Bilawsone
CB	Conduction band
CE	Counter electrode
DFT	Density functional theory
DMSO	Dimethyl sulfoxide
DSSCs	Dye-sensitized solar cells
EA	Electron affinity
E_{ex}	Excitation energy
E_g	Energy gap
ESOP	Excited state oxidation potential
f	Oscillator strength
FF	Fill factor
FTO	Fluorine-doped tin conductive oxide
GAMESS	General atomic and molecular electronic structure system
HOMO	Highest occupied molecular orbital
hv	Photon energy
I_{mp}	Current at maximum power
IP	Ionization potential
IR	Infrared
I_{SC}	Short circuit current
L	Lawsone
LE	Lawsone ether
LUMO	Lowest unoccupied molecular orbital
PCE	Power conversion efficiency
PCM	Polarized continuum model
P_{max}	Maximum power
$\Delta_r E$	Energy of the reaction
$\Delta_r H°(0)$	Enthalpy of the reaction
$\Delta_r H°(T)$	Enthalpy of the reaction at a given temperature

$\Delta_r G°(T)$	Gibbs free energy of the reaction
$\Delta_r S°(T)$	Entropy of the reaction
TD-DFT	Time-dependent density functional theory
UV-Vis	Ultraviolet-visible
V_{mp}	Voltage at maximum power
V_{OC}	Open circuit voltage
η	Efficiency
ε(MO)	Energy of molecular orbital
$\Sigma\omega_{i\ react}$	The sum of the vibration frequencies of the reactants
$\Sigma\omega_{i\ prod}$	The sum of the vibration frequencies of the products

CHAPTER ONE

INTRODUCTION

1.1 Background

Insufficient energy in recent years has become a severe problem worldwide because of the rapid increase in the world population. Today, fossil fuel has been used to power homes and heating (Jamar, Majid, Azmi, Norhafana & Razak, 2016), although it leads to environmental pollutions. Solar energy has become a viable alternative source of energy to fossil fuel due to its unique advantage of green energy and renewable energy. Currently, the energy conversion efficiency of mostly used silicon solar cells has become high and stable (Kong, He, Yan, Zhang & Ju, 2019). However, their energy conversion efficiency does not cut the cost of the materials and cell fabrication (Li, Jingyan, Dixin, Xin & Yanling, 2019) and also the complex purification process of silicon (Kutraleeswaran, Venkatachalam, Saroja, Gowthaman & Shankar, 2017) dramatically limits the further application of such cells.

A dye-sensitized solar cell (DSSC) is a photovoltaic device that converts the visible light into electrical energy through the photoelectrochemical process (De Souza, Deandrade, Müller & Polo, 2018) and has become a viable alternative to silicon solar cells and gained much attention since publication by O'Regan and Grätzel in 1991. The DSSCs are eco-friendly and cost-effective photovoltaic devices which may have relatively high power conversion efficiency (Song *et al.*, 2016; Shinde *et al.*, 2017; Wei *et al.*, 2017). The performance of the DSSCs depends on dye sensitizers, mesoporous semiconductor metal oxide (TiO_2), electrolyte, a counter electrode and photoanode. The dye sensitizer is the molecular pump of DSSCs which is involved in light energy harvesting, regeneration of dye and injection of electrons into the semiconductor; thus the dye plays an essential role in achieving a high power conversion efficiency of the DSSCs (Eshaghi & Aghaei, 2015).

Many researches on DSSCs have been performed; the focus being sensitizers with the highest efficiency for harvesting light. The transition metal compounds ruthenium (II) complexes inorganic dyes anchored to TiO_2 surfaces by using carboxylic acid groups are most successfully used as dye sensitizers showing high power conversion efficiencies of 13% (Mathew *et al.*, 2014) under standard AM 1.5 irradiation. Due to expensiveness, tedious synthesis process and toxicity of metal-based dyes, different investigations have been conducted to find alternative

ways. Synthetic metal-free organic dyes have demonstrated comparatively high efficiency (Zhang *et al.,* 2009; Mathew *et al.,* 2014) close to metal-based dyes but suffering from expensiveness, complicated route of synthesis and low yield.

Plenty of natural dyes extracted from different parts of plants have been examined (Yamazaki *et al.,* 2007; Lim *et al.,* 2015; Syafinar, Gomesh, Irwanto, Fareq & Irwan, 2015; Shinde *et al.,* 2017) owing to their cost-effectiveness, non-toxicity, environmental friendliness and availability. However, the DSSCs based on natural dyes such as lawsone (2-hydroxyl-1,4-naphthoquinone) inherently possess low power conversion efficiency (Chang *et al.,* 2010; Hernandez *et al.,* 2011; Reshak, Shahimin, Juhari & Vairavan, 2013). This compound is used in different area; polymer chemistry, electronics, organic optoelectronics, and anticancer drug fabrication (Zaware, Gonnade, Srinivas, Khan & Rane, 2011; Oda *et al.,* 2018), as well as an electron mediator in biochemical cells (Tanaka, Tamamushi & Ogawa, 1985) and sensitizer in DSSCs (Khadtare *et al.,* 2015). The structural, optoelectronic and other properties of lawsone have been studied experimentally and theoretically (Chemspider, n.d.; Lemmon, McLinden, Friend, Linstrom & Mallard, 2018; Madili, Pogrebnoi & Pogrebnaya, 2018). Previous literature on the performance of lawsone in DSSCs indicated the energy conversion efficiency to be 0.93% (Lakshmi, Krishnakumar, Joseph, Sreelatha & Jinchu, 2016), 0.49% (Al-Bat'hi, Alaei & Sopyan, 2012), as it is seen, the energy conversion efficiency of lawsone is still low.

The present study aimed to modify the lawsone molecule to improve its sensitizing abilities in DSSCs. The lawsone ether (LE) was designed theoretically through a direct combination of two lawsone molecules. The properties of the LE, as well as bilawsone (BL), were studied using quantum chemical methods; the ground state geometries, vibrational and electronic spectra and thermodynamic properties were obtained. Also, UV-Vis spectra of lawsone and bilawsone were measured experimentally. The performances of DSSCs sensitized by lawsone and BL were tested and compared to each other.

1.2 Problem statement

The natural organic dyes such as lawsone (Al-Bat'hi, Alaei & Sopyan, 2012) have been used as alternative photosensitizers to ruthenium-based dye in DSSCs since it generates green energy at low production cost (Preat, Jacquemin & Perpète, 2010). However, the use of single lawsone in DSSCs has been suffered from low light-harvesting and low photovoltaic

conversion efficiency. Therefore, this study intends to modify the lawsone dye molecule in order to broaden the light absorption spectrum and improve its sensitizing abilities in DSSCs.

1.3 Rationale of the study

The use of inorganic dyes, such as ruthenium-based has been proven to have a high photovoltaic efficiency of about 11-13% (Syafinar, Gomesh, Irwanto, Fareq & Irwan, 2015; Lyons *et al.,* 2018) in DSSCs. However, high cost and toxicity of the inorganic dyes (Shalini *et al.,* 2016) limit further applications. The natural dyes have been used as alternative photosensitizers because of high availability, easy to prepare, friendly to the environment, less expensive and non-toxic. Nevertheless, natural dyes exhibit low energy conversion efficiency. Therefore, lawsone based new designed dyes can be potential candidate photosensitizers for increasing photon harvesting, efficient delivering of electrons to the semiconductor metal oxide and improving the photovoltaic conversion efficiency of DSSCs.

1.4 Objectives

1.4.1 General objective

To perform the theoretical design of dyes based on lawsone and experimental measurements of their UV-Vis spectra and DSSCs performance.

1.4.2 Specific objectives

(i) To determine the geometrical structure and spectra of lawsone rotational isomers.

(ii) To design theoretically a lawsone ether (LE) $C_{20}H_{10}O_5$ and determine structural and spectral properties of the lawsone ether and bilawsone (BL).

(iii) To determine the thermodynamic properties of lawsone rotational isomers, lawsone ether and bilawsone.

(iv) To assess the energy conversion efficiency of DSSCs based on the lawsone and bilawsone.

1.5 Research questions

(i) What are the vibrational spectra, structural and electronic spectra of lawsone rotational isomers?

(ii) What are the vibrational spectra, structural and electronic spectra of the lawsone ether and bilawsone?

(iii) What are thermodynamic properties (Gibbs free energies, entropies and enthalpy increments) of the lawsone rotational isomers, lawsone ether and bilawsone?

(iv) What is the energy conversion efficiency of DSSCs based on lawsone and bilawsone?

1.6 Significance of the study

The environmental pollution caused by the use of fossil fuel leads to find an alternative energy source. Today, the use of DSSCs is increasing as an alternative energy source to fossil fuel and high-cost silicon solar cells. The knowledge of the geometrical structures, vibrational spectra, UV-Vis spectra and thermodynamic properties of natural dyes and their derivatives will provide clear direction for their utilization in DSSCs. Furthermore, this study will be used as a base framework for further theoretical and experimental investigations of a new class of organic dyes through a combination of natural dye molecules.

1.7 Delineation of the study

The study was conducted in theoretical and experimental. For the theoretical study, the optimization and vibrational frequencies of all dyes under the study were performed using density functional theory with hybrid functional B3LYP5/6-311G(2d,p). The electronic absorption spectra of molecules in vacuum and solvents (dimethyl sulfoxide (DMSO) and dichloromethane (CH_2Cl_2)) were computed using time-dependent density functional theory. The optimized geometrical parameters and vibrational frequencies were used for calculation of thermodynamic functions of the species in the gas phase: entropies $S°(T)$, reduced Gibbs free energies $\Phi°(T)$, enthalpy increments $H°(T) – H°(0)$. For the experimental study, the UV-Vis absorption spectra of lawsone and bilawsone in DMSO were measured. The performance of dye-sensitized solar cells fabricated with lawsone and bilawsone were tested. The short circuit current I_{SC}, open-circuit voltage V_{OC}, current I and voltage V and solar irradiation G were recorded. The maximum power P_{max}, fill factor FF, and efficiency η were determined.

CHAPTER TWO

LITERATURE REVIEW

2.1 Structure and working principle of dye-sensitized solar cell

Usually, DSSC consists of two electrodes, namely; counter electrode and the working electrode (Fig. 1) which are transparent glass substrates with either thin fluorine-doped tin conductive oxide (FTO) layer or indium doped tin oxide, dye sensitizer and a thin layer of a wide band gap (~3.2 eV) nanocrystalline metal oxide (TiO_2) film pasted onto the working electrode substrate. Because of the wide band gap, TiO_2 semiconductor needs light photons of higher energy (>3.2 eV) which is within near-ultraviolet region to excite electrons from the valence band to the conduction band to generate electricity. Between these two electrodes is placed an electrolyte, usually a solution of potassium iodide/triiodide.

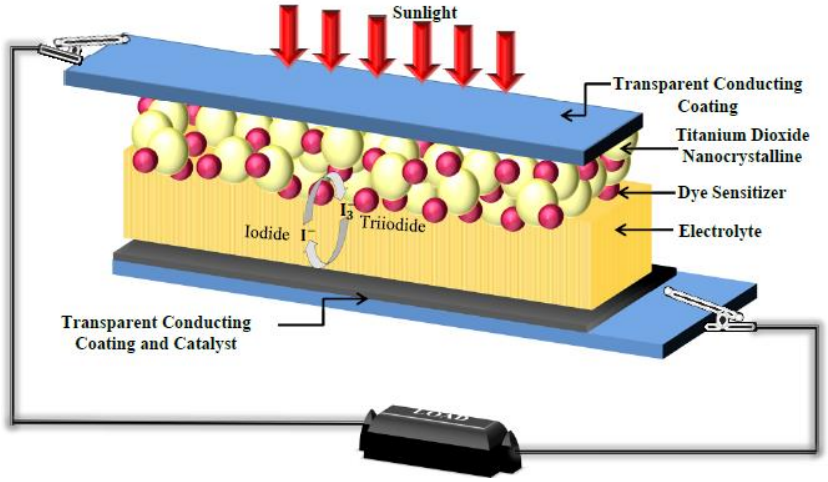

Figure 1. Schematic structure of DSSC (Suhaimi, Shahimin, Chyský & Reshak, 2015).

When the sunlight falls on the cell, light is absorbed by the dye sensitizer on photoanode, generates the excited electrons and electrons are injected into TiO_2 nanoparticles. The injected electrons pass through the conducting electrode (photoanode) and are directed to the load. The dye oxidized is regenerated through reduction from electrolyte (iodide/triiodide), the electrolyte then is regenerated at the counter electrode by getting electrons from an external circuit (Calogero *et al.*, 2014). Working principle of DSSCs is shown in Fig. 2 and summarized in photo-electrochemical reactions in Table 1.

2.2 Basic requirements for efficient photosensitizers

Sensitizers in DSSCs is molecular electron pump (Shalini *et al.*, 2016). The sunlight is absorbed with sensitizers in visible region or near-infrared region and delivers electrons to the conduction band of TiO_2. Many studies on efficient sensitizers have been done showing that best photosensitizers should have the following requirements to improve the performance of the DSSCs. The ability of the dye to harvest light in visible region or near to the infrared region (Rani, Shishodia & Mehra, 2010), the capability of a dye to bind strongly onto the semiconductor surface, successful electron delivering into the conduction band of the semiconductors (Ludin *et al.*, 2014). Also, having an anchoring group namely; hydroxyl, phosphate and carboxylate that are capable of supporting chemical adsorption onto semiconductor of the metal oxide surface to ensure a high rate of electrons transfer (Zhou, Wu, Gao & Ma, 2011), high dye stability is required in ground, and excited state at all temperatures and rapid dye regeneration to avoid electron recombination (Jeon *et al.*, 2014).

Table 1. Photo-electrochemical reactions in DSSCs.

Chemical reaction	Description
$Dye + h\nu \rightarrow Dye^*$	Light absorption
$Dye^* + TiO_2 \rightarrow Dye^+ + e^-_{CB}\ (TiO_2)$	Electron injection
$e^-_{CB}(TiO_2) + C.E. \rightarrow TiO_2 + e^-_{C.E}$ + electrical energy	Energy generation
$2Dye^+ + 3I^- \rightarrow 2Dye + I_3^-$	Dye regeneration
$I_3^- + 2e^-_{catalyst} \rightarrow 3I^-$	Electrolyte regeneration

Calogero, Bartolotta, Dimarco, Dicarlo and Bonaccorso (2015).

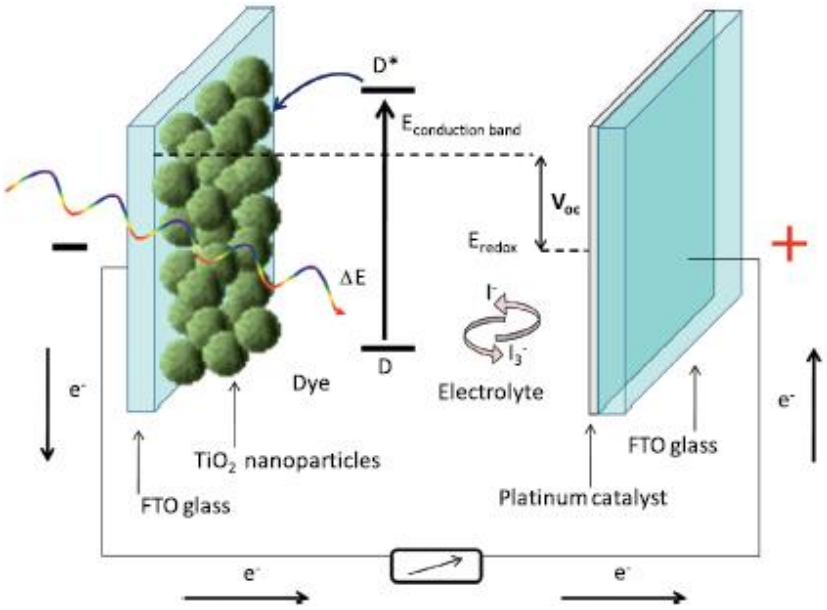

Figure 2. Schematic illustration of working principle of DSSCs (Calogero *et al.*, 2014).

2.3 Energy level alignment

As the working principle of DSSCs states, the sensitizers should have the proper energy level alignment to provide the electrons injection and dye regeneration. Highest occupied molecular orbital (HOMO), lowest unoccupied molecular orbital (LUMO) and energy-gap of photosensitizers should show a potential role in the injection of electrons into a semiconductor. For successful injection of an electron from excited dye to the conduction band of metal oxides, LUMO of the dye should have less negative potential than the conduction band of metal oxide Sinopoli, (Citro, Calogero & Bartolotta, 2017). On the other hand, the HOMO level of the dye must have more negative potential compared to the redox potential of the electrolyte to ensure the oxidized dye could regenerate fast by accepting electrons from the electrolyte (Ananth, Vivek, Kumar & Murugakoothan, 2015).

2.4 Classification of dyes used in dye-sensitized solar cells

The dye plays a crucial role in DSSCs. Based on the requirements mentioned in section 2.2, different types of dyes have been examined, and significant signs of progress in designing sensitizers for DSSCs applications have been made. Generally, dyes are classified as metal-free organic, natural dyes and metal complex (inorganic) dyes as it is seen in Fig. 3.

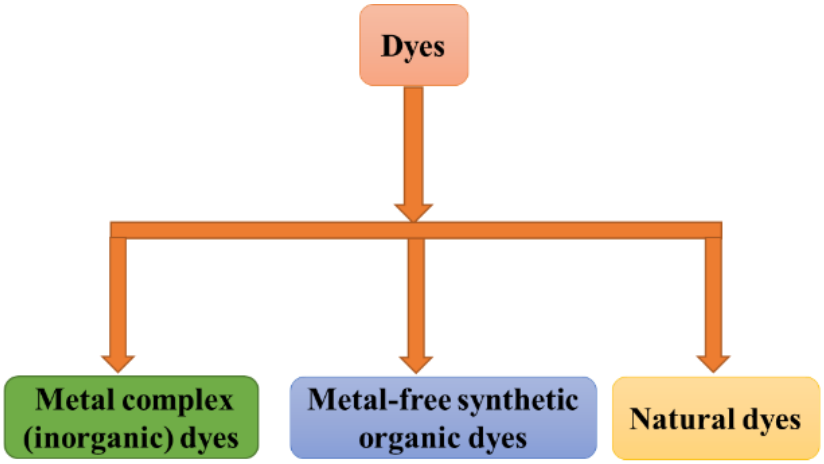

Figure 3. Classification of dyes.

2.4.1 Metal complex (inorganic) dyes

Ruthenium-based complexes are employed as efficient charge-transfer sensitizers, due to their high chemical stability, intense charge transfer absorption in the wide visible range (Hao, Wu, Huang & Lin, 2006) and harvesting ~11-13% solar-to-electric energy in standard global air mass AM 1.5 of sunlight as shown in Table 2. The ruthenium-based complex has functional anchoring groups that are linked to the metal oxides semiconductor. Usually, anchoring groups suitable for metal oxides semiconductor are phosphoric acids H_3PO_4, sulphonic acid (-SO_3H) carboxylic acids (-COOH). Carboxyl groups are often used as anchoring groups which give high efficiency of electrons injection to the semiconductor due to the formation of bidentate-bridging, chelating and ester-linkages with the TiO_2 surface (Calogero, Bartolotta, Dimarco, Dicarlo & Bonaccorso, 2015). However, Ru-complexes are toxic that means not eco-friendly, expensive and also in the presence of water degrade (O'Regan & Grätzel, 1991; Smestad & Gratzel, 1998).

Table 2. Efficiencies of DSSCs based on ruthenium complexes dyes.

Dye	Efficiency, η %	References
N_3	10.3	Calogero, Bartolotta, Dimarco, Dicarlo and Bonaccorso (2015)
	11.18	Nazeeruddin, Baranoff and Grätzel, (2011)
Black Dye	10.4	Nazeeruddin *et al.* (2001)
N719	11.2	Calogero, Bartolotta, Dimarco, Dicarlo and Bonaccorso (2015)
C101	11.3	Gao *et al.* (2008)
C106	9.5	Nguyen *et al.* (2012)
YEO5	10.1	Shelke, Thombre and Patrikar (2017)
N945	10.8	Wang *et al.* (2017)
N712	8.2	Shelke, Thombre and Patrikar (2017)

2.4.2 Metal-free synthetic organic dyes

Metal-free synthetic organic dyes have been used as alternative sensitizers to the Ru-complexes, due to unique advantages; they possess high molar extinction coefficients, efficient light-harvesting capabilities near to the infrared region and eco-friendliness. The performance of the DSSCs sensitized with the synthetic metal-free organic dyes are listed in Table 3.

2.4.3 Natural dyes

Natural dyes contain various pigments that can be extracted from leaves, roots, fruits and flowers and used in DSSCs (Al-Alwani, Mohamad, Kadhum & Ludin, 2015). Benefits of using natural dyes in DSSCs, are that the dyes absorb visible light, electrons are excited and injected into TiO_2. Most significantly, the fabrication method for natural dye-based DSSCs is cost-effective, non-toxic and eco-friendly. Despite the low cost of the natural dyes, most of them do not yield high energy conversion efficiency. The photovoltaic performance of the DSSCs based on natural dyes sensitizers is shown in Table 4.

Table 3. Efficiencies of DSSCs based on metal-free synthetic organic dyes.

Dye	Efficiency, η %	References
C217	9.8	Calogero, Bartolotta, Dimarco, Dicarlo and Bonaccorso (2015)
D205	9.4	Calogero, Bartolotta, Dimarco, Dicarlo and Bonaccorso (2015)
RK1	10.2	Calogero, Bartolotta, Dimarco, Dicarlo and Bonaccorso (2015)
D102	6.1	Ogura *et al.* (2009)
D149	7.1	Ogura *et al.* (2009)
D131	5.6	Ogura *et al.* (2009)
TA-ST-CA	9.1	Calogero, Bartolotta, Dimarco, Dicarlo and Bonaccorso (2015)
TA-DM-CA	9.7	Calogero, Bartolotta, Dimarco, Dicarlo and Bonaccorso (2015)

Table 4. Efficiencies of DSSCs based on natural dyes.

Dye Solution	Efficiency, η (%)	References
Lawsone	0.93	Lakshmi, Krishnakumar, Joseph, Sreelatha and Jinchu (2016)
″	0.56	Khadtare *et al.* (2015)
″	0.52	Aduloju, Shitta and Justus (2011)
″	0.20	Das, Gogoi and Chowdhury (2018)
Purple Cabbage	0.75	Suhaimi, Shahimin, Alahmed, Chyský and Reshak (2015)
Begonia	0.24	Zhou, Wu, Gao and Ma (2011)
Tangerine Peel	0.28	Zhou, Wu, Gao and Ma (2011)
Crocetin	0.56	Yamazaki *et al.* (2007)
Lawsone	0.05	Madili, Pogrebnoi and Pogrebnaya, (2018)
Lycopene.	0.55	Shinde *et al.* (2017)
Red Bougainvillea Spectabilis	0.48	Hernandez *et al.* (2011)
Spinach	0.13	Chang *et al.* (2010)

2.5 Molecular design

The design of the new dye sensitizer can be done through a combination of one dye component with another capable of increasing the energy conversion efficiency of the solar cells. Msangi, Pogrebnoi and Pogrebnaya (2018), designed a new dye theoretically through a combination of natural dye (crocetin) and synthetic dye (indoline D205). The results showed that the designed complex had widened light absorption in a visible range compared to individual dyes. Because of the high cost of the synthetic dye, our study will be focused on cost-effective natural dye lawsone through which lawsone ether 2-(1,4-dihydro-1,4-dioxonaphthalen-3-yloxy) naphthalene-1,4-dione (LE) will be designed theoretically. The structural and optoelectronic properties of the lawsone, designed LE, as well as bilawsone (BL), will be determined. Below in Fig. 4 there are structural formulae of lawsone $C_{10}H_6O_3$, lawsone ether $C_{20}H_{10}O_5$ and bilawsone $C_{20}H_{10}O_6$.

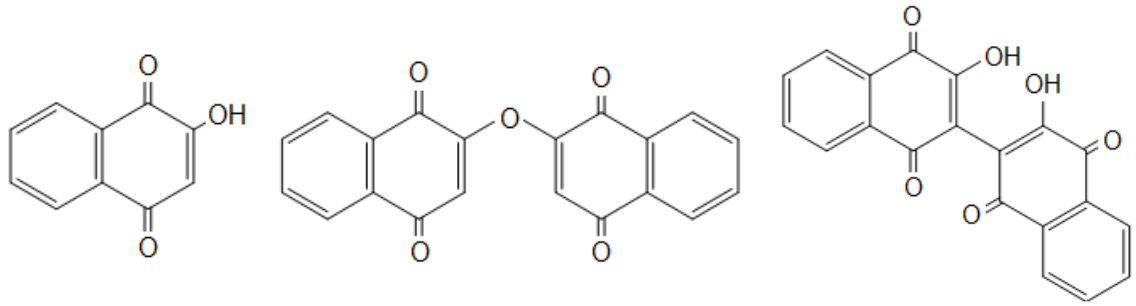

L, lawsone: 2-hydroxyl-1,4-naphthoquinone

LE, lawsone ether: 2-(1,4-dihydro-1,4-dioxonaphthalen-3-yloxy) naphthalene-1,4-dione

BL, bilawsone: 2,2-Bi(3-hydroxy-1,4-naphthoquinone

Figure 4. Structural formulae of lawsone, lawsone ether and bilawsone.

CHAPTER THREE

MATERIALS AND METHODS

3.1 Computational details

The initial molecular geometry of lawsone (L) was taken from the National Institute of Standards and Technology (NIST) database (Lemmon *et al.*, 2018) and for BL was taken from ChemSpider database (chemspider, n.d.); Avogadro software (Hanwell *et al.*, 2012) was used to construct the input files for quantum chemical computations. The structures were optimized without imposing any geometrical constraints. The geometry optimization of the molecules was performed using density functional theory (DFT) with hybrid functional B3LYP5 (Vosko, Wilk & Nusair, 1980; Lee, Yang & Parr, 1988) and basis set 6-311G(2d,p). The B3LYP5 functional provides reliable results for structural parameters and optical properties for organic molecules computations. The computation of frequencies was carried out with the same method and ensured the obtained structures corresponded to the minima on the potential energy surfaces. The electronic absorption spectra of the molecules in a vacuum, dimethyl sulfoxide (DMSO) and dichloromethane (CH_2Cl_2) were simulated using time-dependent density functional theory (TD-DFT) with the B3LYP5/6-311G(2d,p). The solvent effect was evaluated based on the polarizable continuum model (PCM) (Cossi, Scalmani, Rega & Barone, 2002). All calculations were performed using the Firefly QC package which partially based on the general atomic and molecular electronic structure system (GAMESS) US source code (Schmidt *et al.*, 1993). The Chemcraft (Zhurko & Zhurko, 2015) and MacMolPlt (Bode & Gordon, 1998) software were used to visualize and analyze the geometrical structures, vibrational and electronic spectra of the considered dye molecules.

The optimized geometrical parameters and vibrational frequencies were used for calculation of thermodynamic functions of the species in the gas phase: entropies $S°(T)$, reduced Gibbs free energies $\Phi°(T)$, enthalpy increments $H°(T) - H°(0)$ which were calculated within 'rigid rotor-harmonic oscillator' approximation by means of OpenThermo software. Energies of the reactions $\Delta_r E$ are obtained through total energies of products and reactants:

$$\Delta_r E = \Sigma E_{prod} - \Sigma E_{react} \quad (1)$$

The enthalpies of the reactions $\Delta_r H^o(0)$ are calculated as follows:

$$\Delta_r H°(0) = \Delta_r E + \Delta_r \varepsilon \quad (2)$$

$\Delta_r\varepsilon$ is zero-point vibration energy (ZPVE),

$$\Delta_r \varepsilon = \frac{1}{2} hc\left(\sum \omega_{i\,prod} - \sum \omega_{i\,react}\right) \quad (3)$$

where *h* represents the Planck's constant, *c* is the speed of light in the free space, $\sum \omega_{i\,prod}$ and $\sum \omega_{i\,react}$ is the sum of the vibration frequencies of the products and reactants, respectively. The enthalpies, $\Delta_r H°(T)$, Gibbs free energies $\Delta_r G°(T)$ and entropies $\Delta_r S°(T)$ of the reactions at a given temperature are computed with the following classical thermodynamics equations:

$$\Delta_r H°(T) = \Delta_r H°(0) + \Delta_r[H°(T) - H°(0)] \quad (4)$$

$$\Delta_r G°(T) = \Delta_r H°(T) - T\Delta_r S°(T) \quad (5)$$

3.2 Experimental details

3.2.1 Materials and chemicals

Lawsone and bilawsone of 97% purity were commercially purchased from Sigma-Aldrich and Career Henan Co, respectively. Also, the solvent, dichloromethane (CH_2Cl_2) and dimethyl sulfoxide (DMSO) were purchased from Sigma-Aldrich. Test cell kit with chemicals includes chenodeoxycholic acid, ruthenium N_3 dye, iodolyte AN-50, Vac'n'Fill Syringe, titania electrodes and platinum electrodes were purchased from Solaronix company (Switzerland). The purchased chemicals were used without further purifications for the solutions preparations. Electric furnace, ammeter, resistors, connecting wires, multimeters and solar power meter obtained from NM-AIST laboratory. The UV-Vis spectrophotometer was kindly provided for measurements by Arusha Technical Research Centre (ATRC).

3.2.2 Measurement of UV-Vis absorption spectra

The solutions of concentration 0.038 g/L for lawsone and 0.027 g/L for bilawsone were prepared by dissolving 3.8 mg (lawsone) and 2.7 mg (bilawsone) both in 100 mL of DMSO. The UV-Vis absorption spectra of the dyes in DMSO have recorded automatically in the range 200-700 nm by using Jenway spectrophotometer UK 6715 V1.42 model.

3.2.3 Fabrication of dye-sensitized solar cell

Dye-Sensitized Solar Cell (DSSC) was assembled adopting the methods by Madili, Pogrebnoi and Pogrebnaya (2018). Titania electrodes (photoanode) were re-activated at 450 °C for 10 minutes in the electric furnace and then left to cool naturally in the air. Activated TiO_2 was immersed in the 0.038 g/L lawsone in DMSO solution at ambient temperature for 24 h to obtain ultimately staining. The dyed TiO_2 electrodes were taken out from the lawsone solution and rinsed with ethanol to remove loosely dye on TiO_2 and then placed in air to allow ethanol to evaporate to leave TiO_2 electrodes dried. Platinum electrodes (counter electrodes) were re-activated at 450 °C for 10 minutes, then cooled naturally in the air. Then the counter electrode was placed on the top of sensitized photoanode so that the conductive side of the counter electrode faced the TiO_2 film. The iodide electrolyte solution (Iodolyte AN-50) was poured at the edge of electrodes. Electrodes were held together with two binder clips. The fabrication process of DSSCs is summarized in Fig. 5. Therefore, the DSSCs were ready for characterization. The same procedures were repeated for bilawsone solution (0.027 g/L).

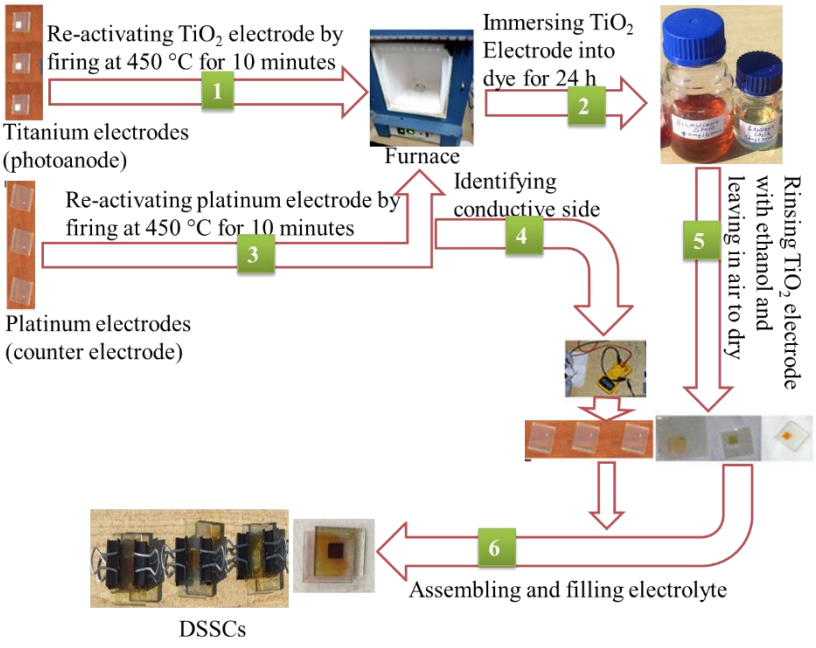

Figure 5. The fabrication process of DSSCs.

3.2.4 Testing the performance of dye-sensitized solar cells

The outdoors experiment of the photoelectrical performance for the DSSCs was done. The active surface area A for each tested DSSC was 36 mm^2. The DSSC was connected in series with an ammeter and resistor and parallel with voltmeter using connecting wires as shown in Figs. 6–7. The short circuit current I_{SC} was measured when resistance was zero and open-circuit voltage V_{OC} was measured when the current (I) reached zero at maximum resistance. The current I and voltage V were recorded by varying the resistance while solar irradiation G was recorded using the solar power meter. The graphs of I-V and power P-V were plotted. The maximum power P_{max}, fill factor FF, and efficiency η were calculated using the following equations:

$$P_{max} = I_{mp}\, V_{mp} \tag{6}$$

$$FF = \frac{I_{mp}\, V_{mp}}{I_{SC} V_{OC}} \tag{7}$$

$$\eta = \left(\frac{P_{max}}{P_{in}}\right) = \frac{I_{mp}\, V_{mp}}{AG} \tag{8}$$

where I_{mp} is current at maximum power, V_{mp} is the voltage at maximum power, A is the active surface area of titanium electrode and P_{in} is power input.

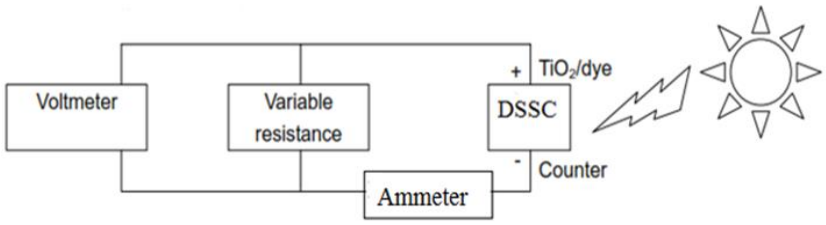

Figure 6. The schematic diagram for DSSCs performance.

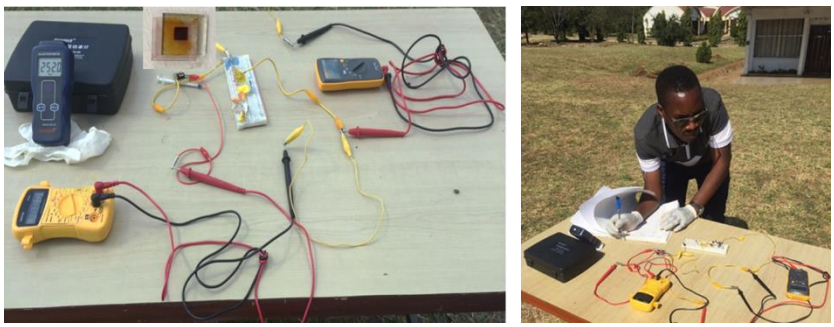

Figure 7. Experimental setup for outdoor measurement.

CHAPTER FOUR

RESULTS AND DISCUSSION

4.1 Lawsone rotational isomers

4.1.1 Geometrical structure

Two rotational lawsone isomers, L′ and L, were considered (Fig. 8). Both geometrical structures are planar, the L isomer being more stable by ~30 kJ mol^{-1}. The higher stability of the L is attributed to the formation of the intramolecular hydrogen bond; this result is in agreement with literature data (Hanna, Nowak, Lipinski & Adamowich, 1998; Todkary *et al.*, 2006; Pawar, Jadhav, Wadekar & Sarawadekar, 2011; Vessecchi, Emery, Galembeck & Lopes, 2012) where the existence of intramolecular hydrogen bond in lawsone molecule also was reported. The selected geometrical parameters of the L′ and L are compared between each other and also with experimental X-ray diffraction data (Todkary *et al.*, 2006) as shown in Table 5.

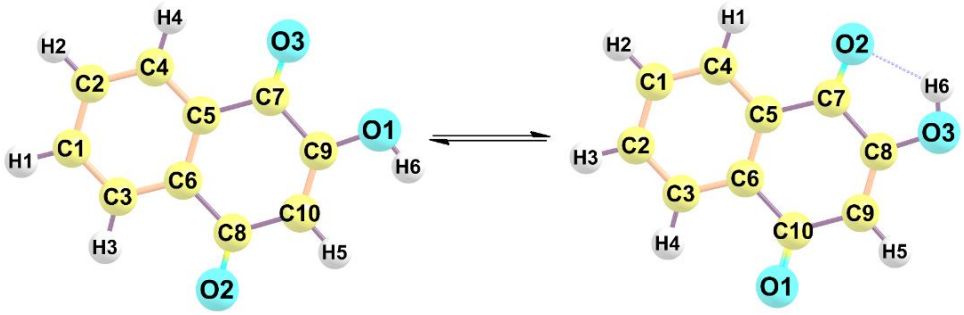

Figure 8. Optimized geometrical structures of lawsone rotational isomers L′ and L.

The most noticeable difference between the L′ and L is seen for parameters which relate to the rotating O-H group; maximum elongation of bond lengths is 0.012 Å (O-H), shrinkage –0.014 Å (C-C), bond angles are reduced by 3° (C-C-O) and 4° (C-O-H). Other geometrical parameters remain virtually unchangeable. Worth to note that our structural characteristics, in general, agree well with the X-ray diffraction experimental data of crystal phase (Todkary *et al.*, 2006).

Table 5. Selected geometrical parameters of lawsone rotational isomers L′ and L.

L′		L		Difference	Expt. (Todkary *et al.*, 2006)
		Bond length, Å			
C9-O1	1.342	C8-O3	1.334	–0.008	1.334
C9-C7	1.504	C8-C7	1.497	–0.007	1.506
C7=O3	1.212	C7=O2	1.223	+0.011	1.211
C9=C10	1.347	C8=C9	1.347	0.000	1.322
C7-C5	1.486	C7-C5	1.472	–0.014	1.501
C10-C8	1.464	C9-C10	1.462	–0.002	1.412
C8=O2	1.220	C10=O1	1.220	0.000	1.230
C8-C6	1.495	C10-C6	1.503	+0.008	1.502
C1-H1	1.086	C2-H3	1.084	–0.002	0.930
C5=C6	1.401	C5=C6	1.403	+0.002	1.386
O1-H6	0.967	O3-H6	0.979	+0.012	0.820
		Bond angle, deg			
O1-C9-C7	112.8	O3-C8-C7	113.9	+1.1	114.4
O1-C9-C10	125.4	O3-C8-C9	123.9	–1.5	124.8
C9-C7-O3	120.4	C8-C7-O2	117.4	–3.0	120.4
C10-C8-O2	121.1	C9-C10-O1	121.4	+0.3	123.1
O2-C8-C6	121.5	O1-C10-C6	120.6	–0.9	118.2
C9-C10-C8	122.5	C8-C9-C10	121.2	–1.3	122.6
C10-C9-C7	121.8	C9-C8-C7	122.2	+0.4	122.2
O3-C7-C5	123.0	O2-C7-C5	124.4	+1.4	123.1
C9-O1-H6	109.5	C8-O3-H6	105.3	–4.2	109.5
C9-C7-C5	116.6	C8-C7-C5	118.2	+1.6	116.4
C7-C5-C4	119.1	C7-C5-C4	120.2	+1.1	121.1
C4-C5-C6	119.9	C4-C5-C6	120.4	+0.5	119.6
C2-C4-C5	119.9	C1-C4-C5	119.7	–0.2	121.1
C3-C6-C5	119.8	C3-C6-C5	119.5	–0.3	119.2
C3-C6-C8	119.6	C3-C6-C10	119.6	0.0	120.1

4.1.2 Vibrational spectra

The theoretical vibrational spectra of the L′ and L molecules are compared in Fig. 9 between each other. Bands at 3790 cm^{-1} for L′ and 3580 cm^{-1} for L correspond to stretching vibrations of the hydroxyl group; the decrease of the frequency is due to H-bond formation in L and accords with the elongation of the O-H bond from 0.967 Å to 0.979 Å, respectively (Table 5). The small peaks at ~3180 cm^{-1} are assigned to the C-H bond stretching in the aromatic and aliphatic rings. The most intensive sharp peaks at 1720–1750 cm^{-1} are attributed to the stretching vibrations of carbonyl C=O groups. The peaks at 1660–1630 cm^{-1} are assigned to C=C stretching vibrations in the benzenoid and quinoid rings; the bending vibrations C–O-H at ~1320 cm^{-1}, C-C-H ~1250 cm^{-1} and C-H out of plane 1000–500 cm^{-1} are observed. The vibrational frequencies obtained theoretically here comply with typical frequencies of the respective functional groups. The calculated spectrum of L appeared to be in a good agreement with the experimental IR spectrum of lawsone in the gas phase (Ananth, Vivek, Arumanayagam & Murugakoothan, 2014; Lemmon *et al.*, 2018).

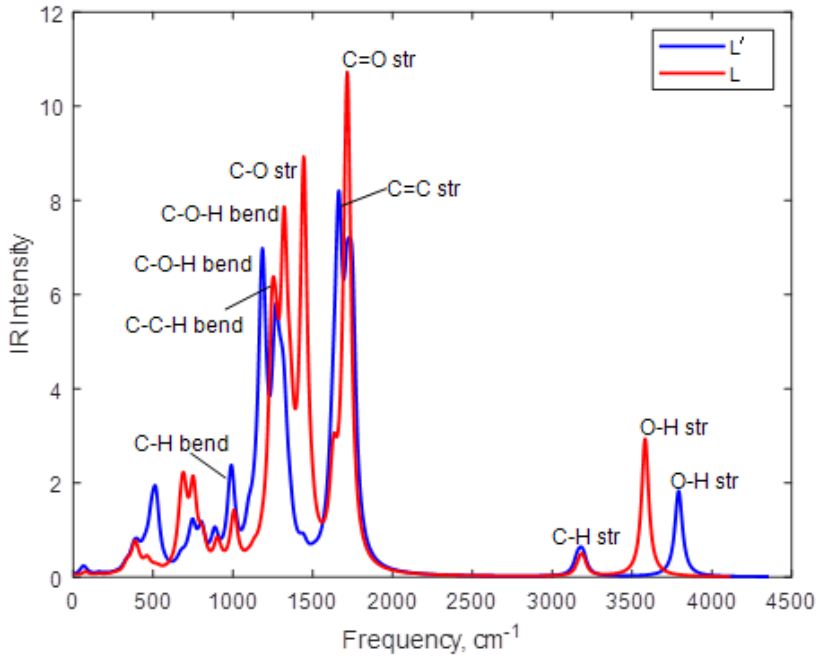

Figure 9. Infrared region (IR) spectra of the L′ and L molecules.

4.1.3 Thermodynamics of isomerization reaction

For the isomerization reaction

$$L' \leftrightarrow L, \quad (I)$$

thermodynamic characteristics were calculated using equations (1)–(5). The values of enthalpies, $\Delta_r H°(0) = -30.0$ kJ mol^{-1}, $\Delta_r H°(298) = -30.6$ kJ mol^{-1}, entropy $\Delta_r S°(298) = -4.5$ J mol^{-1} K^{-1}, and Gibbs free energy $\Delta_r G°(298) = -29.2$ kJ mol^{-1} were obtained. The results show that the reaction is exothermic and spontaneous at ambient conditions. To evaluate which isomer was predominant the equilibrium constant $K°_p(T)$ of isomerization reaction (I) was also calculated for the temperature range between 298 K and 600 K using equations:

$$\Delta_r H°(0) = T[\Delta_r \Phi°(T) - R\ln K°_p(T)] \quad (9)$$

$$\Phi°(T) = -\left[\frac{[H°(T) - H°(0)] - TS°(T)}{T}\right] \quad (10)$$

where $\Delta_r \Phi°(T)$ represents the reduced Gibbs free energy of the reaction at a given temperature. The results are presented in Fig. 10 and indicate that the equilibrium constant is much greater than 1; it decreases by three orders with temperature increase, from 1.3×10^5 (298 K) to 2.5×10^2 (600 K); hence the isomer L is predominant in the temperature range considered. From the slope of the plot, the enthalpy of the isomerization reaction is $\Delta_r H°(400\ K) = -30.8$ kJ mol^{-1} that is there was no significant change in this value when temperature increased. The Gibbs free energies $\Delta_r G°(T)$ were also calculated (Fig. 13) and proved the reaction remain exergonic in the broad temperature interval. The thermodynamic functions of the species are listed in Table A in the Appendix.

In further sections, the most stable isomer L is considered as the reactant in the lawsone ether and bilawsone formation as well as in electronic spectra and molecular orbitals analyses.

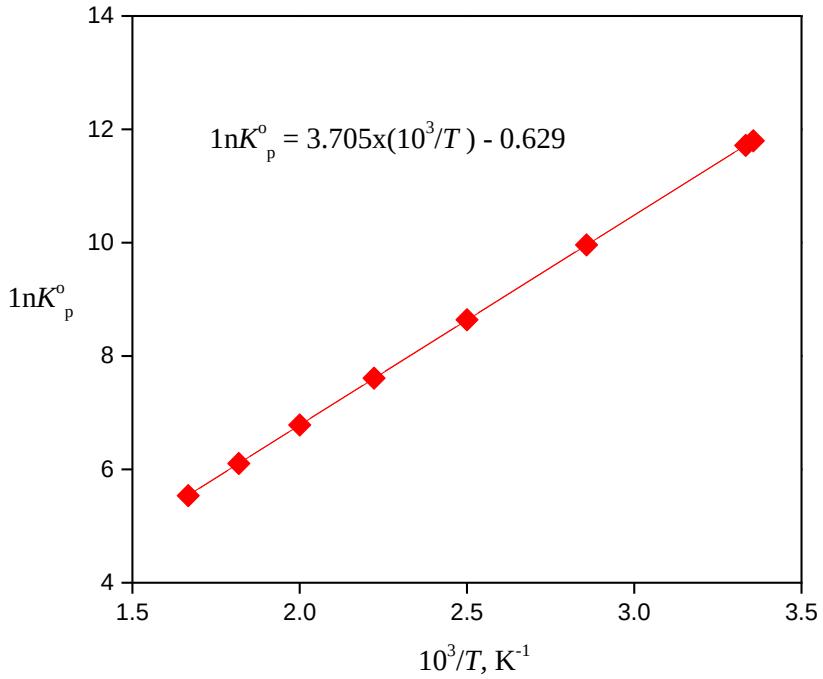

Figure 10. Temperature dependence of the equilibrium constant of the isomerization reaction L′ ↔ L.

4.2 Lawsone ether and bilawsone

4.2.1 Geometrical structure

A combination of two lawsone molecules L is considered as etherification reaction with the lawsone ether $C_{20}H_{10}O_5$ and elimination of water:

$$2C_{10}H_6O_3 \rightarrow C_{20}H_{10}O_5 + H_2O \qquad \text{(II)}$$

According to IUPAC nomenclature, the name of the designed LE molecule is 2-(1,4-dihydro-1,4-dioxonaphthalen-3-yloxy) naphthalene-1,4-dione. The other direct combination of two L molecules leads to bilawsone $C_{20}H_{10}O_6$ formation, hydrogen being detached:

$$2C_{10}H_6O_3 \rightarrow C_{20}H_{10}O_6 + H_2 \qquad \text{(III)}$$

The optimized geometrical structures of the LE and BL are shown in Fig. 11; both molecules contain one symmetry element, C_2 rotation axis; thus, the structures belong to the C_2 point group symmetry. The selected geometrical parameters of LE and BL are compared between each other and with L in Table 6.

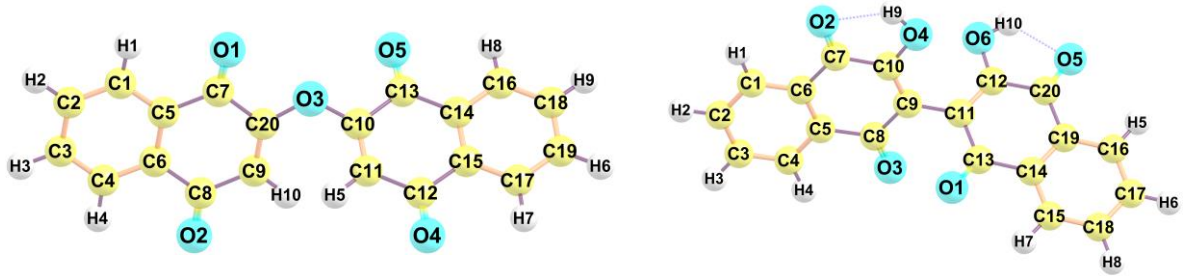

LE BL

Figure 11. The optimized geometrical structures of the LE and BL molecules.

In the LE, the linkage C10-O3-C20 between two lawsone moieties is specified with parameters R_e(O3-C10) = R_e(O3-C20) = 1.358 Å and ∠C10-O3-C20 = 125°. The LE molecule is propeller-shaped due to lawsone fragments are turned one to another by 52°. In the vicinity of the linkage, the bond lengths of carbonyl groups C7=O1 and C13=O5 are reduced by 0.012 Å, whereas the other two, C8=O2 and C12=O4, remained very close to respective bonds in L. The bond angles ∠O3-C10-C13 = ∠O3-C20-C7 in LE are reduced by 2.2° while ∠C10-C13=O5 = ∠C20-C7=O1 in LE are increased by 3.0° compared to respective angles, ∠O3-C8-C7 and ∠C8-C7=O2, in monomer lawsone.

In the BL, the link C9-C11 is formed between two L moieties with R_e = 1.476 Å. Similarly to the LE, the BL structure is non-planar with the angle between two L 62°. A noticeable change is observed in the vicinity of the linkage; the R_e(C8-C9) = R_e(C11-C13) is longer by 0.015 Å than R_e(C9-C10) in L. The parameters of the distant parts of the LE and BL practically coincide with those in the lawsone molecule; the benzene rings remain planar, while quinoid rings exhibit a slight non-planarity.

4.2.2 Vibrational spectra

Theoretical IR spectra of the LE and BL molecules are shown in Fig. 12; the spectrum of the lawsone is given for comparison. The higher band intensities of LE and BL are apparently attributed to greater in the number of atoms and hence more IR active vibrations compared to L. The most intensive sharp peaks at 1232 cm^{-1} (LE) and 1420 cm^{-1} (BL) are assigned to C-O stretching vibrations. The increase of vibrational frequency is in line with the decrease of the C-O bond length from 1.358 Å (LE) to 1.332 Å (BL). Worth to note that peak 1232 cm^{-1} in LE corresponds to the link C-O-C between two L-moieties and that band represents a unique

vibration of the LE IR spectrum which allows distinguishing the ether among the three molecules.

The peaks at 3570 cm^{-1} in BL and 3580 cm^{-1} in L are attributed to stretching vibrations of free hydroxyl groups O-H. The small peaks at 3180–3190 cm^{-1} in L, LE and BL are assigned to C-H stretching vibrations in the benzenoid rings. The stretching vibrations of the carbonyl groups C=O are observed at 1720–1750 cm^{-1} (LE) and 1720 cm^{-1} (BL, L). The C=C stretching vibrations are seen as intensive peak 1646 cm^{-1} in LE and small peak 1690 cm^{-1} in BL. The bending vibrations C-C-C and C-C-O are observed at 1300–1360 cm^{-1} as a very high peak in BL and low peak in L but not exhibited at all in IR spectrum of the ether. In general, the wavenumbers found theoretically for the molecules under study accord with typical vibrational frequencies of respective functional groups (Pavia, Lampman & Kriz, 2001).

Table 6. Selected geometrical parameters of LE, BL and L.

LE		BL		L	
Bond length, Å					
C10-O3, C20-O3	1.358	C10-O4, C12-O6	1.332	C8-O3	1.334
C10-C13, C20-C7	1.504	C10-C7, C12-C20	1.495	C7-C8	1.497
C7=O1, C13=O5	1.211	C7=O2, C20=O5	1.232	C7=O2	1.223
C20=C9, C10=C11	1.342	C9=C10, C11=C12	1.353	C8=C9	1.347
C5-C7, C13-C14	1.486	C6-C7, C19-C20	1.470	C5-C7	1.472
C8=O2, C12=O4	1.219	C8=O3, C13=O1	1.220	C10=O1	1.220
C5-C6, C14-C15	1.408	C5-C6, C14-C19	1.405	C5-C6	1.403
		C9-C11	1.476		
C8-C9, C11-C12	1.473	C8-C9, C11-C13	1.477	C9-C10	1.462
Bond angle, deg					
O3-C10-C13, O3-C20-C7	111.7	O4-C10-C7, O6-C12-C20	113.3	O3-C8-C7	113.9
O3-C10=C11, O3-C20=C9	126.0	O4-C10=C9, O6-C12=C11	123.7	O3-C8-C9	123.9
C10-C13=O5, C20-C7=O1	120.4	C10-C7=O2, C20-C12=O5	117.1	C8-C7-O2	117.4
C9-C8=O2, C11-C12=O4,	120.3	C9-C8=O3, C11-C13=O1	121.2	C9-C10-O1	121.4
C7-C5-C1, C13-C14-C16	119.1	C1-C6-C7, C16-C19-C20	120.4	C4-C5-C7	120.2
		C8-C9-C11, C13-C11-C9	119.7		
C8-C9-C20, C10-C11-C12	121.9	C8- C9-C10, C12-C11-C13	119.5	C8-C9-C10	121.2
Dihedral angle, deg					
C2-C3-C9-C20	0.5	C2-C3-C9-C10	0.5	C1-C2-C9-C8	0.0
C9-C20-C10-C11	52.2	C10-C9-C11-C12	62.0		
C6-C5-C14-C15	56.1	C6-C5-C14-C19	72.1		

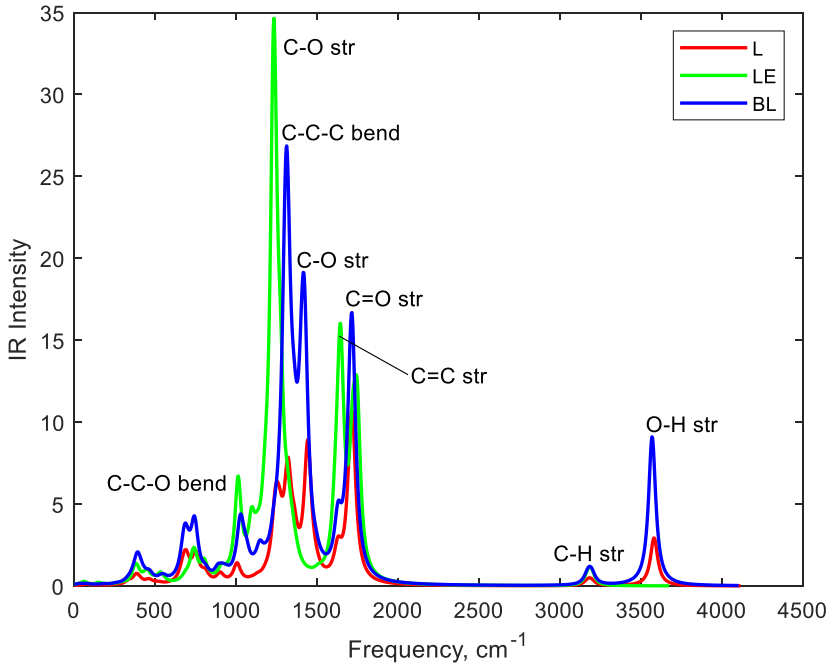

Figure 12. IR Spectra of L, LE and BL.

4.2.3 Thermodynamics of reactions

Thermodynamic characteristics of the reactions (II) and (III) were computed using equations (1)-(5) and listed in Table 7. The values of $\Delta_r H°(298)$ and $\Delta_r G°(298)$ are positive; this implies that the reactions are endothermic and non-spontaneous at room temperature.

Table 7. Thermodynamic characteristics of chemical reactions.

Reaction	$\Delta_r E$	$\Delta_r \varepsilon$	$\Delta_r H°(0)$ kJ mol^{-1}	$\Delta_r H°(298)$	$\Delta_r S°(298)$ J mol^{-1} K^{-1}	$\Delta_r G°(298)$ kJ mol^{-1}
$2C_{10}H_6O_3 \rightarrow C_{20}H_{10}O_5 + H_2O$	109.7	–12.86	96.9	104.2	–2.7	105.0
$2C_{10}H_6O_3 \rightarrow C_{20}H_{10}O_6 + H_2$	57.8	–26.58	31.2	38.8	–63.3	57.7

Temperature dependences of thermodynamic characteristics of the reactions (I)-(III) are presented in Fig. 13. The values of $\Delta_r H°(T)$, and $\Delta_r G°(T)$ remain positive for the LE and BL formation reactions in a broad temperature range. Thus these two reactions are endothermic and endergonic that is in contrast to the lawsone isomerization reaction (I). As concerns entropy, the values $\Delta_r S°(T)$ are rather small for reactions (I) and (II) and do not contribute much to the Gibbs free energies. The entropy of reaction (III) is negative with a great numerical value that implies a distinctive ordering of the BL. The BL structure seems less flexible due to the rigidity of the C-C bond as compared to C-O-C link in LE, and that is confirmed by greater bending frequency of two lawsone fragments in BL (26 cm^{-1}) than in LE (11 cm^{-1}). The flexibility of C-O-C connection in LE allows more freedom for structural rearrangement in contrast to BL in which short C-C link brings to the hindered motion of the moieties, thus to sufficient entropy decrease. With temperature rise, the value of $\Delta_r S°(T)$ for reaction (III) changes visibly, from –63 J mol^{-1} K^{-1} at 300 K to –46 J mol^{-1} K^{-1} at 600 K (Fig. 13b), that results in a noticeable increase of Gibbs free energy (Fig. 13c).

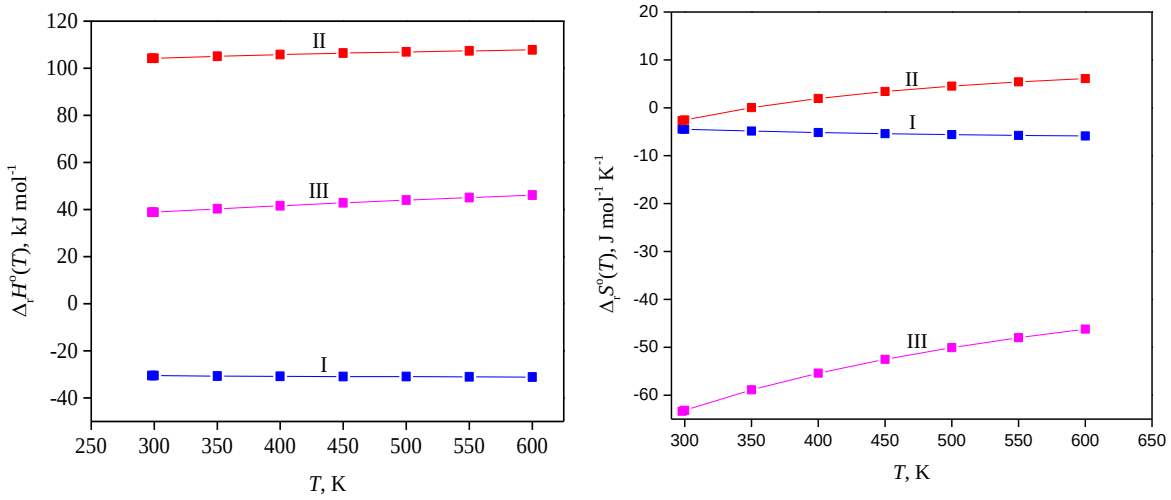

(a) (b)

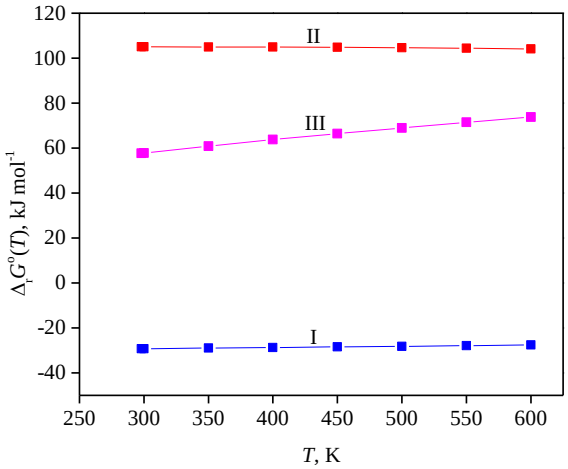

(c)

Figure 13. Temperature dependence of thermodynamic characteristics of reactions (I)–(III): (a) $\Delta_r H°(T)$, (b) $\Delta_r S°(T)$ and (c) $\Delta_r G°(T)$.

4.3 Optoelectronic properties

4.3.1 Electronic spectra

The light absorption spectrum of a dye is of importance for evaluating its light-harvesting capability and efficiency of DSSCs. Electronic spectra of dyes under study have been computed for vacuum and solvents (dimethyl sulfoxide and dichloromethane), the singlet-singlet $S_0 \rightarrow S_n$ (n = 1-10) excitations with non-zero oscillator strength ($f > 0.001$) are taken into account. Absorption properties of a dye may be specified in terms of light-harvesting efficiency (LHE).

The LHE values at a particular wavelength are calculated through the following expression (Gélinas *et al.*, 2014; Lee & Kim, 2016).

$$\text{LHE} = 1 - 10^{-f} \tag{9}$$

The excitation energies (E_{ex}), wavelengths (λ), oscillator strengths (*f*), LHE, electronic transition configurations are summarized in Table 8. The theoretical UV-Vis spectra of the molecules for vacuum and DMSO are presented in Fig. 14.

Table 8. Electronic transitions $S_0 \rightarrow S_n$ (n = 1-10) in L, LE and BL computed for vacuum and solutions.

Excited state, No.	E_{ex}, eV	λ, nm	*f*	LHE	Electronic transition configuration[a]
L in vacuum					
4	3.79	327	0.056	0.12	H-2 → L (91%)
5	4.39	282	0.155	0.30	H-3 → L (86%)
7	5.19	239	0.173	0.33	H → L+1 (81%)
9	5.66	219	0.027	0.06	H-3 → L+1 (68%)
L in DMSO					
4	3.65	340	0.059	0.13	H-2 → L (93%)
5	4.33	287	0.167	0.32	H-3 → L (90%)
7	5.30	234	0.217	0.39	H → L+1 (86%)
9	5.73	217	0.004	0.01	H-3→L+1 (67%)
10	5.78	215	0.027	0.06	H-2 → L+1 (77%)
L in CH_2Cl_2					
4	3.67	338	0.059	0.13	H-2 → L (93%)
5	4.33	286	0.166	0.32	H-3 → L (89%)
7	5.30	234	0.211	0.39	H → L+1 (86%)
9	5.71	217	0.005	0.01	H-3→L+1 (67%)
10	5.79	214	0.027	0.06	H-2 → L+1 (78%)
LE in vacuum					
3	3.05	406	0.006	0.01	H-6 → L (47%)
5	3.20	387	0.045	0.10	H → L (71%)
7	3.64	342	0.083	0.17	H-3 → L (48%)
8	3.64	340	0.003	0.01	H-4 → L (42%)
9	3.67	338	0.002	0.01	H-3 → L (40%)
LE in DMSO					
3	3.04	408	0.038	0.08	H → L (90%)
5	3.22	385	0.004	0.01	H-7 → L (55%)
7	3.47	357	0.089	0.19	H-2 → L (44%)
9	3.58	346	0.016	0.04	H-4 → L (62%)
LE in CH_2Cl_2					
3	3.05	406	0.037	0.08	H → L (87%)
7	3.50	355	0.088	0.18	H-2 → L (46%)
9	3.61	344	0.016	0.04	H-4 → L (43%)

Excited state, No.	E_{ex}, eV	λ, nm	*f*	LHE	Electronic transition configuration[a]
BL in vacuum					
1	2.75	451	0.062	0.13	H→ L (81%)
3	2.86	434	0.027	0.06	H-1 → L (56%)
4	2.93	424	0.003	0.01	H → L+1 (59%)
8	3.52	352	0.002	0.01	H-3 → L+1 (67%)
10	3.63	341	0.014	0.03	H-8 → L (44%)
BL in DMSO					
1	2.76	448	0.064	0.14	H → L (95%)
2	2.87	431	0.002	0.01	H → L+1 (87%)
3	2.98	416	0.005	0.01	H-3 → L (63%)
6	3.43	361	0.003	0.01	H-1 → L+1 (28%)
8	3.52	352	0.096	0.20	H-4 → L (48%)
9	3.57	348	0.022	0.05	H-4 →L (31%) H-2 → L+1 (22%) H-5 → L+1 (21%)
10	3.58	346	0.010	0.02	H-5 → L (49%)
BL in CH_2Cl_2					
1	2.77	448	0.067	0.14	H → L (95%)
2	2.87	432	0.003	0.01	H → L+1 (85%)
3	2.96	418	0.006	0.01	H-2 → L (66%)
8	3.53	352	0.066	0.14	H-3 → L+1 (53%)
9	3.58	346	0.051	0.11	H-4 → L (56%)
10	3.60	345	0.009	0.02	H-5 → L (59%)

[a] H and L represent HOMO and LUMO, respectively.

For the lawsone both in a vacuum and solutions, the most probable transitions are seen in UV region of the spectrum, they occur from the ground state to the fifth and seventh excited states and assigned mostly to the H-3→L and H→L+1 MOs, respectively. The excitations in the visible range are available but of low probability. From vacuum to the solution, slight red shit is observed for longer wavelengths transitions, while the blue shift for shorter (Fig. 14a). Both for LE and BL, the lowest energy excitations (with λ_{max}) are generally in the visible part of the spectrum and belong to the most probable transitions which correspond commonly to H→L MOs. As is seen from Table 8, there is no significant difference in the results obtained for two solvents, DMSO and CH_2Cl_2. Therefore the solvent effect on the spectra is considered mostly for the former in the next sections.

The highest absorption peaks of LE are observed at 342 and 387 nm in a vacuum, 357 and 408 nm in DMSO; thus, the LE exhibits red-shift in solutions compared to vacuum (Fig. 14b). In the theoretical UV-Vis spectra of BL (Fig. 14c), the highest intensity peaks are seen at 341 and 451 nm (vacuum) and 352 and 448 nm (DMSO), thus no evident red or blue shift is observed

for BL. While considering the spectra of the three compounds (Fig. 14d), in a visible range, the LE and BL possess peaks of higher intensity and strongly shifted to longer wavelengths region compared to L, that should favour sensitizing performance of the complex molecules.

Experimental UV-Vis spectra of L and BL in DMSO solution are presented in Fig. 15. For the lawsone, the simulated spectrum (Fig. 14a) agrees well with the experiment (Fig. 15a) regarding peaks position and intensities. Also, our results are in accordance with UV-Vis spectra of lawsone measured earlier (Mahkam, Kafshboran & Nabati, 2014; Khadtare *et al.*, 2015; Madili, Pogrebnoi & Pogrebnaya, 2018) as well as theoretical data obtained in (Jacquemin, Preat, Wathelet & Perpète, 2006; Madili, Pogrebnoi & Pogrebnaya, 2018).

In the experimental spectrum of the BL (Fig. 15b), a broad and intensive band is observed in a visible range (452 nm), that indicates a good sensitizing ability of the dye. Theoretical values of λ, 448 nm and 352 nm (Fig. 14b), agree well with peaks position in the experiment. The number of excited states was extended up to 25 in the simulated spectrum of the BL to attain the ultraviolet region; the transitions at 288 259 and 248 nm were obtained in addition, which agrees well with respective bands position of the measured spectrum. To best of our knowledge, no experimental study of the UV-Vis spectrum of bilawsone was reported up to now.

The calculated LHE values are rather low, that is in accordance with literature data for natural dyes (Sun, Li, Song & Ma, 2016; Liu, Ren, Wang, Li & Yang, 2018; Zhao, Lu, Su, Li & Zhao, 2019). As seen, the LHEs of L are higher compared to the LE and BL, but the light absorption of L occurs in UV-region which does not favour sensitizing ability, while for LE and BL the simulation predicts the absorption in the visible range, hence better DSSCs performance.

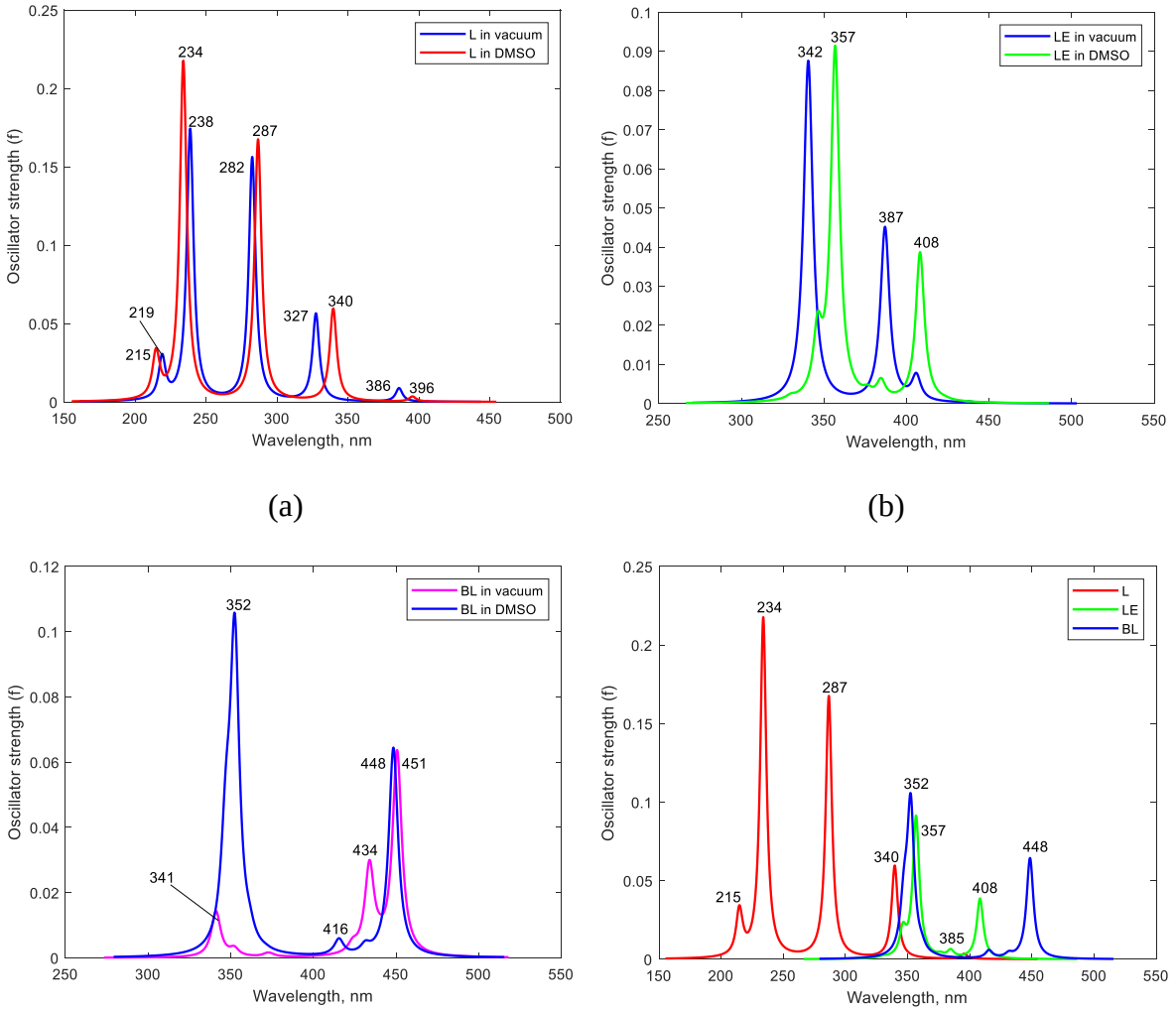

Figure 14. Theoretical UV-Vis spectra of molecules in a vacuum and DMSO: (a) L, (b) LE, (c) BL and (d) comparison between L, LE and BL in DMSO.

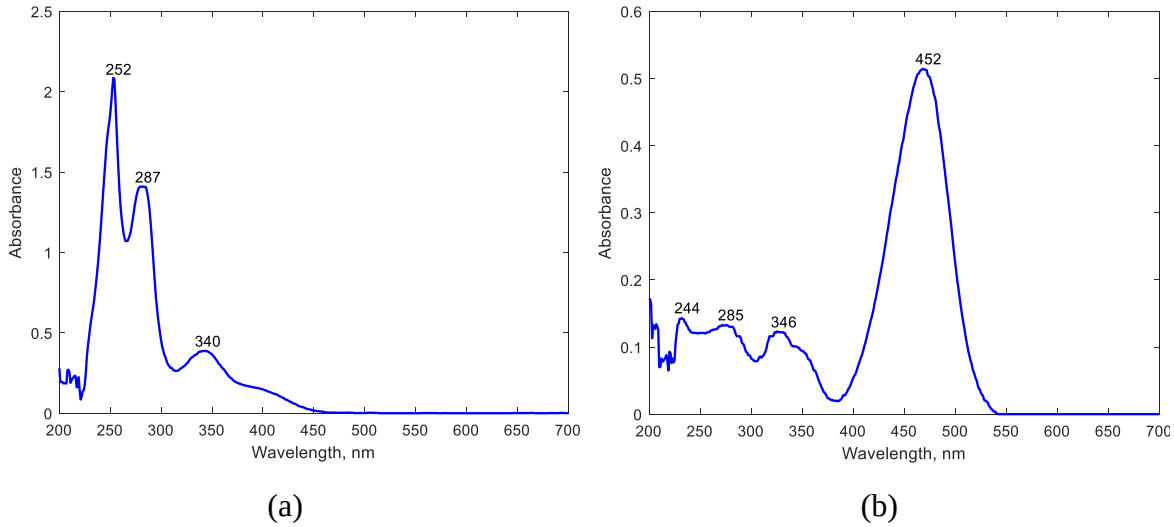

Figure 15. UV-Vis spectra measured experimentally in DMSO: (a) L, (b) BL.

4.3.2 Molecular orbitals analysis

The MO analysis provides information about the electronic structure of molecules and potential electron transitions (Msangi, Pogrebnoi & Pogrebnaya, 2018). For the L, LE and BL, the frontier and adjacent MOs which mostly participate in the electron excitations are selected as computed for DMSO solutions (Table 8); isosurfaces of these MOs are shown in Fig. 15. For the lawsone, the electron density distributions in the HOMO-3, HOMO-2, HOMO, LUMO, and LUMO+1 are presented (Fig. 16a). The most probable excitation with the highest *f* value and wavelength 287 nm is assigned to the HOMO-3→LUMO. The transition at 340 nm is attributed to HOMO-2→LUMO and that at 234 nm to HOMO→LUMO+1. The electron density of the occupied MOs is mainly concentrated on the benzenoid ring, whereas that of unoccupied orbitals is on the quinoid ring; thus the $\pi \rightarrow \pi^*$ transitions involve electron delocalization from the benzenoid to quinoid ring.

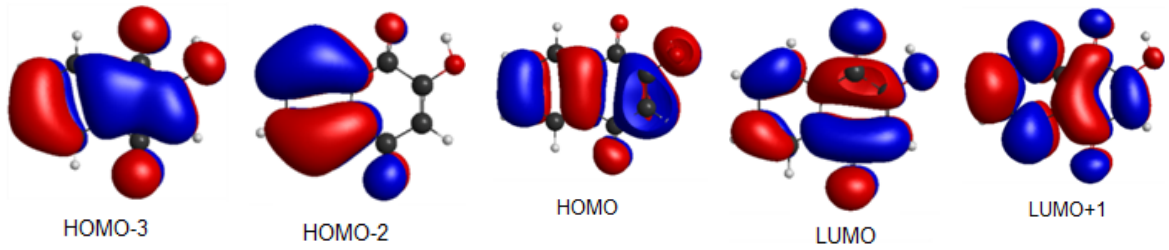

(a) L

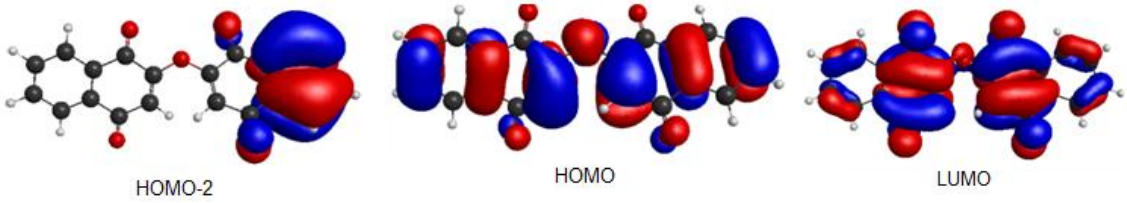

(b) LE

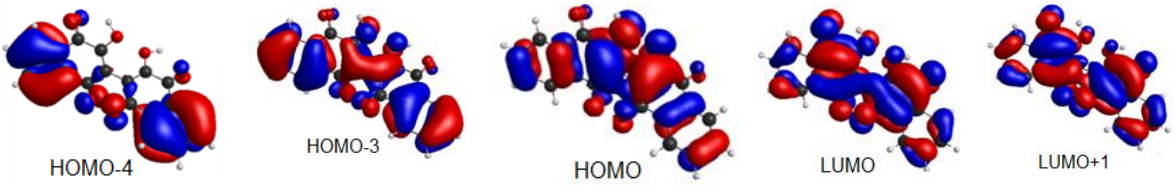

(c) BL

Figure 16. Frontier and adjacent MOs of the species in DMSO: (a) L; (b) LE and (c) BL.

For the LE, the isosurfaces of the HOMO-2, HOMO and LUMO are shown in Fig. 16b. The maximum wavelength absorption in the visible region at 408 nm arises from the HOMO→LUMO transition. The electron density of HOMO is delocalized over the π-system on benzenoid and quinoid rings, whereas that of LUMO is mostly located on the quinoid ring. In the highest oscillator strength transition, $f = 0.089$ and $\lambda = 357$ nm, which is assigned mainly to HOMO-2→LUMO, the electron density shifts from the benzenoid to quinoid rings.

For the BL, the HOMO-4, HOMO, LUMO, and LUMO+1 (Fig. 16c) are involved in the significant electronic excitations. In the HOMO→LUMO transition observed at 448 nm, the electrons in HOMO are delocalized across the entire molecular structure, whereas those in LUMO are concentrated more in the quinoid rings. In the most probable transition, $f = 0.096$ and $\lambda = 352$ nm, assigned to HOMO-4→LUMO, the electrons density is redistributed from benzenoid to quinoid rings.

Summarizing the MO analysis some common features may be noticed for three species L, LE and BL. As for the MOs which are below HOMO, the electron density is concentrated mostly on the benzenoid rings; while in HOMOs, the electrons are delocalized across the molecule. Regarding the unoccupied MOs, the electron density is located in the quinoid rings predominantly. Worth to mention about the electron transitions of highest probabilities in the LE HOMO-2→LUMO and in BL HOMO-4→LUMO for which spatial separation of electron densities between occupied and free MOs is observed (Figs. 16b, c). Therefore that separation leads to increase of the exciton size and hence favours higher stability of the electron-hole couples formed, which in turn results in hindering recombination processes and improving sensitizing properties of the dyes.

Moreover, it might be suggested that oxygen atoms of the quinone moieties are anchoring groups to attach titanium atoms (anchoring sites) of the TiO_2 semiconductor. To facilitate the intermolecular charge transfer, the appropriate arrangement between the dye and substrate is important. It appeared that the interatomic distances O-O in LE and BL accord well with the Ti-Ti distances in the TiO_2 rutile crystal: in the LE, O1-O5 = 4.64 Å, O2-O4 = 6.53 Å are close to $a = 4.60$ Å, $a\sqrt{2} = 6.50$ Å in the TiO_2, respectively; also in the BL, O1-O3 = 3.05 Å is near to $c = 2.96$ Å. The lattice parameters of the TiO_2 have been taken from (Howard, Sabine & Dickson, 1991). Thus, from the compliance between the substrate and verisimilar anchoring

O-atoms accompanied with the suitable electron density location, the LE and BL are considered to surpass the L dye in sensitizing performance in DSSCs.

4.3.3 Energy levels alignment

The overall power conversion efficiency of DSSCs depends on the proper energy level alignment of a dye to ensure good electrons injection and dye regeneration (Li, Jingyan, Dixin, Xin & Yanling, 2019). The simplest way to consider this alignment is to draw the frontier MOs energy levels with valence and conduction band edge of a substrate as well as redox level of electrolyte. It is more appropriate to represent excited states via excited states oxidation potentials (ESOPs) (Oprea, Frecuş, Minaev & Girtu, 2011; Madili, Pogrebnoi & Pogrebnaya, 2018) which have been obtained as the sum of the occupied energy levels and relevant excitation energies. The calculated energies of frontier and adjacent MOs, excitation energies E_{ex}, energy gaps E_g, and ESOPs, are listed in Table 9. The results indicate that the values of E_g exceed the respective excitation energies systematically: the difference $E_g - E_{ex}$ is in the range 0.20–1.07 eV; that brings to the lowering of the ESOPs compared to respective unoccupied MOs.

The energy level diagram of most relevant MOs of the species in solutions is shown in Fig. 17; along with the LUMO energies, ESOPs are also given. According to a good photosensitizer requirement, a LUMO of a dye should lie slightly above the conduction band edge of the semiconductor TiO_2 (–4.05 eV (Fujisawa, Eda & Hanaya, 2017)) to ensure electrons injection into the substrate from the excited dye; and HOMO should lie under the redox potential of the electrolyte I^-/I_3^- (–4.80 eV (Zhang *et al.*, 2009)) for dye regeneration by accepting electrons from the electrolyte. As is observed in Fig. 17 all three molecules meet criteria of energy level alignment to be appropriate photosensitizers for TiO_2 semiconductor due to LUMO levels lie above the conduction band of TiO_2, the ESOPs approach very close to the CB edge, permitting electron transfer to the substrate. The HOMO levels lie below the redox level of the I^-/I_3^- electrolyte allowing electron transfer to the pigment molecule from the electrolyte.

Table 9. Energies of molecular orbitals ε(MO), excitation energies E_{ex}, energy gaps E_g and ESOPs; all values are in eV.

MO	ε(MO)	Transition	E_{ex}	E_g	ESOP
L in vacuum					
43, H-2	–7.59	H-2 → L	3.79	4.38	–3.80
42, H-3	–7.84	H-3 → L	4.39	4.63	–3.45
45, H	–7.12	H → L+1	5.19	5.73	–1.93
46, L	–3.21				
47, L+1	–1.39				
L in DMSO					
45, H	–7.15	H → L	3.13	3.87	–4.02
43, H-2	–7.49	H-2 → L	3.65	4.22	–3.84
42, H-3	–7.80	H-3 → L	4.33	4.53	–3.47
46, L	–3.27	H → L+1	5.30	5.85	–1.85
47, L+1	–1.30				
L in CH_2Cl_2					
45, H	–7.15	H → L	3.15	3.89	–4.00
43, H-2	–7.51	H-2 → L	3.67	4.25	–3.84
42, H-3	–7.80	H-3 → L	4.33	4.54	–3.47
46, L	–3.26	H → L+1	5.30	5.85	–1.85
47, L+1	–1.31				
LE in vacuum					
85, H	–7.27	H → L	3.20	3.84	–4.07
82, H-3	–7.61	H-3 → L	3.64	4.18	–3.97
86, L	–3.43				
LE in DMSO					
85, H	–7.28	H → L	3.04	3.74	–4.24
83, H-2	–7.54	H-2 → L	3.47	4.00	–4.07
81, H-4	–7.61	H-4 → L	3.58	4.07	–4.03
86, L	–3.54				
LE in CH_2Cl_2					
85, H	–7.28	H → L	3.05	3.75	–4.23
83, H-2	–7.55	H-2 → L	3.50	4.02	–4.05
86, L	–3.53				
BL in vacuum					
89, H	–6.60	H→ L	2.75	3.38	–3.85
88, H-1	–7.15	H-1 → L	2.86	3.93	–4.29
90, L	–3.22				
BL in DMSO					
89, H	–6.85	H → L	2.76	3.41	–4.09
85, H-4	–7.53	H-4 → L	3.52	4.09	–4.01
86, H-3	–7.47	H-3 → L+1	3.53	4.25	–3.94
90, L	–3.44				
BL in CH_2Cl_2					
89, H	–6.81	H → L	2.77	3.40	–4.04
86, H-3	–7.49	H-3 → L+1	3.54	4.26	–3.95
85, H-4	–7.52	H-4 → L	3.58	4.11	–3.94
90, L	–3.41				
91, L+1	–3.23				

The excitation energies have a significant effect on the efficiency of DSSCs; sensitizer with lower excitation energies are advantageous to electron excitation and that facilitates light absorption in the long-wavelength range. The LE and BL exhibit smaller excitation energies (2.76, 3.52, and 3.53 eV) and (3.04, 3.47, 3.58 eV) compared to the individual lawsone (3.79, 4.39, 5.19 eV). Therefore, these results indicate that the LE and BL are better photosensitizers candidates for DSSCs compared to the natural lawsone pigment.

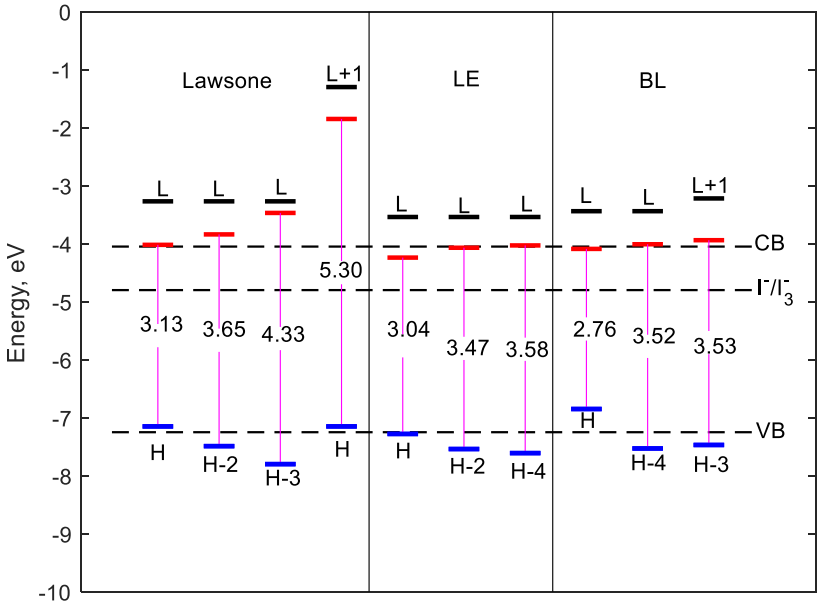

Figure 17. Energy level diagram of most relevant MOs, ESOPs (red bars) and excitation energies for lawsone, lawsone ether and bilawsone in solvents.

4.3.4 Ionization potentials and electron affinities

The ionization potential (IP) and electron affinity (EA) directly depict the energy barrier of the hole and electron injection to the conduction band of TiO_2 (Li, Jingyan, Dixin, Xin & Yanling, 2019; Zanjanchi & Beheshtian, 2019). The IP and EA can be calculated by using the following equations:

$$\mathrm{IP} = E_{\mathrm{cation}} - E_{\mathrm{neutral}} \tag{11}$$

$$\mathrm{EA} = E_{\mathrm{neutral}} - E_{\mathrm{anion}} \tag{12}$$

In this work, the IP or EA is taken as difference between the energies of the reference ground state and open-shell ionized form when the electron is removed or added. The calculated values of IP and EA are given in Table 10 and compared with HOMO and LUMO energies, respectively. As is seen, the IP for each dye is higher compared to HOMO by 1.4-2.0 eV and

EA is lower compared to LUMO by 1.3-1.9 eV; this indicates that the magnitudes of IPs and EAs do not coincide with corresponding MOs energies. This discordance may be explained as follows. According to the Koopmans' theorem, minus HOMO energy is assumed to equal the IP (and similarly for LUMO and EA). Apparently, the frontier MOs' energies depend on theoretical approach implemented. In our work, the DFT/B3LYP5 method has been used; and the Kohn–Sham respective MOs eigenvalues appeared to differ from IP or EA. This disadvantage of the DFT/B3LYP approach is rather common and has been also noticed earlier, see for example (Zhang & Musgrave, 2007). As for experimental measurements, only for the lawsone molecule the IP and EA are available in literature; worth to note that the calculated IP for L appeared to be in a good agreement with the experimental value (Millefiori, Gulino & Casarin, 1990).

Table 10. Ionization potentials, electron affinities and frontier MOs energies of L, LE and BL

Dye	IP	ε(HOMO)	EA	ε(LUMO)	Experimental	
					IP	EA
L	9.17	–7.12	1.38	–3.22	9.20[a]	1.85[b]
LE	8.69	–7.27	2.06	–3.43		
BL	8.11	–6.60	1.83	–3.20		

[a] Millefiori *et al.* (1990) and [b] Asfandiarov *et al.* (2014).

4.4 Photovoltaic properties of dye-sensitized solar cells

Photovoltaic properties of DSSCs sensitized with lawsone and bilawsone under the sunlight irradiance of 1248 ±10 W m^{-2} and 1450 ±10 W m^{-2} respectively are shown in Fig. 18a-b. In all fabricated DSSCs the active area was 36 mm^2. The short circuit current, open-circuit voltage, maximum power, fill factor and power conversion efficiency of DSSCs are listed in Table 11. The curves *I-V* and *P-V* plotted show the features typical for photovoltaic devices.

The performance of the DSSCs fabricated with lawsone was tested: the electrical parameters were measured: 3.0 μA short-circuit current, 140.0 mV open-circuit voltage and 270.7 μW maximum power. For bilawsone based DSSC, higher values were obtained: 10.0 μA short-circuit current, 160.0 mV open-circuit voltage and 865.1 μW power maximum. Moreover, bilawsone dye shows the photo conversion efficiency of the DSSC η = 1.7% that is higher compared to 0.6% of individual lawsone sensitizer. These results of efficiencies are in accordance with the theoretical expectation of the optoelectronic properties of the dyes.

Table 11. Photovoltaic parameters of DSSCs based on lawsone and bilawsone.

Dye	G, W m^{-2}	V_{OC}, mV	I_{SC}, µA	I_{mp}, µA	V_{mp}, mV	P_{max}, µW	FF, %	η, %	Reference
Lawsone	1248	140.0	3.0	2.7	98.8	270.7	64.5	0.60	This study
Lawsone	1000	520	1.8	-	-	-	62.0	0.56	Khadtare *et al.* (2015)
Lawsone	1000	590	1.4	-	-	-	65.0	0.52	Aduloju *et al.*, (2011)
Bilawsone	1450	160.0	10.0	7.9	109.2	865.1	54.5	1.70	This study

The efficiency of lawsone obtained is comparable to the efficiencies 0.56% and 0.52% reported by Khadtare *et al.* (2015) and Aduloju *et al.* (2011) respectively. Regarding the bilawsone, the improved photovoltaic performance of DSSCs might be due to the presence of two hydroxyl groups (OH) as auxochrome and anchoring groups adsorbed firmly to the TiO_2 semiconductor which leads to better charge transfer to the semiconductor. Also, OH provides the extended conjugation in the molecule, which leads to intensive absorption at 452 nm.

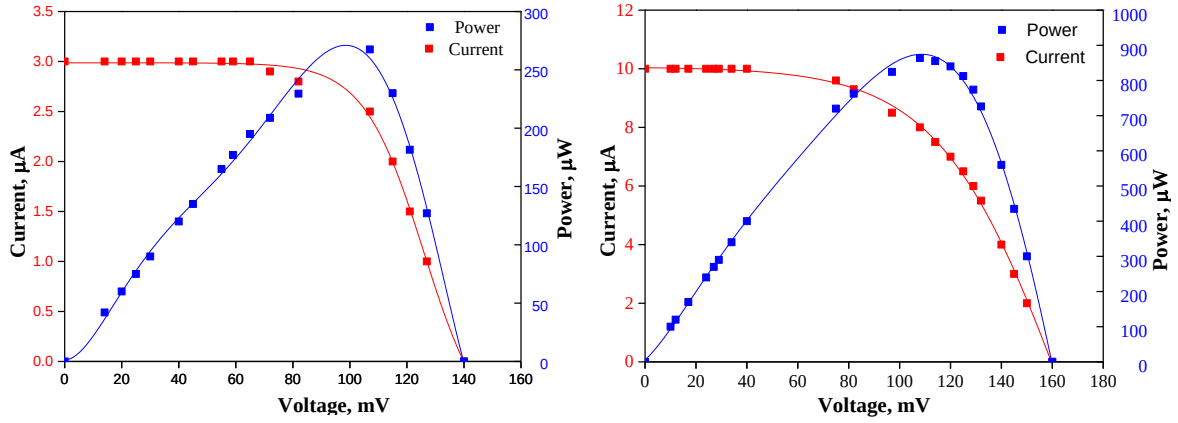

(a) (b)

Figure 18. *I-V* and *P-V* curves for DSSC sensitized with (a) L and (b) BL.

CHAPTER FIVE

CONCLUSION AND RECOMMENDATIONS

5.1 Conclusion

The lawsone, lawsone ether and bilawsone sensitizers were studied theoretically, and also the experimental studies of lawsone and bilawsone dyes solutions were performed on the UV-Vis spectra measurements together with fabrication of the DSSCs and testing their performances.

Structural parameters, thermodynamic properties, IR and UV-Vis spectra of the lawsone, lawsone ether and bilawsone were studied. Two rotational isomers of the lawsone molecule were considered, and that one with the intramolecular hydrogen bond appeared to dominate in equilibrium vapour. The combination of two lawsone molecules resulting in either lawsone ether or bilawsone was proposed. The thermodynamic approach indicated that the direct reactions of LE and BL formation were endothermic and non-spontaneous.

Optoelectronic properties of the L, LE and BL were studied; the results obtained demonstrated that the LE and BL possessed better light-harvesting and sensitizing abilities compared to lawsone due to their lower excitation energies, intense absorption bands in the visible range and higher electron-hole couple stability. The theoretical UV-Vis spectra of lawsone and bilawsone were in accordance with experimental spectra. The UV-Vis spectrum of bilawsone was measured and reported here for the first time. It is suggested that the bilawsone and lawsone ether are promising photosensitizers for DSSCs.

Based on the measurements of *I-V* and *P-V* curves of fabricated dye-sensitized solar cells, the short circuit current, maximum power, open-circuit voltage, fill factor, and power conversion efficiency were determined. The DSSCs sensitized with bilawsone have shown higher efficiency (1.7%) compared to that for lawsone (0.6%) which might be explained by the presence of two OH-groups bringing to extended conjugation and broadening visible range in the adsorption spectra. Also the OH-groups might favour stronger binding between the dye and TiO_2 semiconductor which cause successful injection of electrons in semiconductor. Therefore, the energy conversion efficiency of the cell using bilawsone dye revealed the enhancement in the cell performance.

5.2 Recommendations

The sensitizers – lawsone, lawsone ether and bilawsone – have been investigated by using the quantum chemical methods and are predicted to be suitable photosensitizer for DSSCs. The big challenge of the DSSC is low power conversion efficiency. Therefore, to enhance the performance of the DSSCs the following recommendations can be suggested:

(i) Further improvement of the dyes sensitizing properties, the design of molecules by grafting of anchoring groups may be suggested to facilitate the charge transfer and bonding to the semiconductor surface.

(ii) Also, further computational studies on dye-semiconductor interaction are recommended to investigate charge transfer properties and binding stability onto the semiconductor metal oxides.

(iii) Investigation of aging of the DSSCs with the L, LE and BL dyes due to dye degradation.

Experimental synthesis of designed lawsone ether through etherification reaction of two lawsone molecules and characterizations such as FTIR, ^{1}H NMR and ^{13}C NMR are recommended.

Computational studies on juglone 5-hydroxy-1,4-naphthoquinone and naphthoquinone derivatives are recommended to be done. Also, investigation on how different anchoring groups and different position of OH-groups affect the optoelectronic properties lawsone, bilawsone, juglone and naphthoquinone derivatives.

REFERENCES

Aduloju, K. A., Shitta, M. B., & Justus, S. (2011). Effect of extracting solvents on the stability and performances of dye-sensitized solar cell prepared using extract from Lawsonia Inermis. *Fundamental Journal of Modern Physics*, *1*(2), 261-268. Retrieved from http://erepository.uonbi.ac.ke/bitstream/handle/11295/37169/EFFECT%20OF%20EXTRACTING%20SOLVENTS%20ON%20THE%20STABILITY.pdf?sequence=1

Al-Alwani, M. A., Mohamad, A. B., Kadhum, A. A. H., & Ludin, N. A. (2015). Effect of solvents on the extraction of natural pigments and adsorption onto TiO_2 for dye-sensitized solar cell applications. *Spectrochimica Acta Part A: Molecular Biomolecular Spectroscopy*, *138*, 130-137. doi: 10.1016/j.saa.2014.11.018

Al-Bat'hi, S. A., Alaei, I., & Sopyan, I. (2012). Natural Dye Photosensitizers/Solid State Electrolyte Junction for Dssc Application: *The European Workshop and Conference on Renewable Energy Systems*. (pp. 1-7). Antalya, Turkey.

Ananth, S., Vivek, P., Arumanayagam, T., & Murugakoothan, P. (2014). Natural dye extract of Lawsonia inermis seed as a photosensitizer for titanium dioxide based dye sensitized solar cells. *Spectrochimica Acta Part A: Molecular Biomolecular Spectroscopy*, *128*, 420-426. doi: 10.1016/j.saa.2014.02.169

Ananth, S., Vivek, P., Kumar, G. S., & Murugakoothan, P. (2015). Performance of Caesalpinia sappan heartwood extract as photo sensitizer for dye sensitized solar cells. *Spectrochimica Acta Part A: Molecular Biomolecular Spectroscopy*, *137*, 345-350. doi: 10.1016/j.saa.2014.08.083

Asfandiarov, N., Pshenichnyuk, S., Vorob'Ev, A., Nafikova, E., Elkin, Y., Pelageev, D., . . . Modelli, A. (2014). Electron attachment to some naphthoquinone derivatives: long-lived molecular anion formation. *Rapid Communications in Mass Spectrometry*, *28*(14), 1580-1590. doi: 10.1002/rcm.6934

Bode, B. M., & Gordon, M. S. (1998). MacMolPlt version 7.4.2. *Journal of Molecular Graphics and Modelling*, *16*(3), 133-138. doi: 10.4236/oalib.1101978

Calogero, G., Bartolotta, A., Di Marco, G., Di Carlo, A., & Bonaccorso, F. (2015). Vegetable-based dye-sensitized solar cells. *Chemical Society Reviews*, *44*(10), 3244-3294. doi: 10.1039/C4CS00309H

Calogero, G., Citro, I., Di Marco, G., Minicante, S. A., Morabito, M., & Genovese, G. (2014). Brown seaweed pigment as a dye source for photoelectrochemical solar cells. *Spectrochimica Acta Part A: Molecular Biomolecular Spectroscopy*, *117*, 702-706. doi: 10.1016/j.saa.2013.09.019

Chang, H., Wu, H., Chen, T., Huang, K., Jwo, C., & Lo, Y. (2010). Dye-sensitized solar cell using natural dyes extracted from spinach and ipomoea. *Journal of Alloys Compounds*, *495*(2), 606-610. doi: 10.1016/j.jallcom.2009.10.057

Chemspider. (n.d.). Retrieved from http://www.chemspider.com

Cossi, M., Scalmani, G., Rega, N., & Barone, V. (2002). New developments in the polarizable continuum model for quantum mechanical and classical calculations on molecules in solution. *The Journal of Chemical Physics*, *117*(1), 43-54. doi: 10.1063/1.1480445

Das, S., Gogoi, K. K., & Chowdhury, A. (2018). Fabrication of dye sensitized solar cell using natural plant pigment as sensitizers. *America Institute of Physics Conference Proceedings*, *1998*(1), 020016-1-020016-6. doi: 10.1063/1.5049112

De Souza, J., De Andrade, L. O. M., Müller, A. V., & Polo, A. S. (2018). Nanomaterials for solar energy conversion: dye-sensitized solar cells based on ruthenium (II) Tris-heteroleptic compounds or natural dyes. *Nanoenergy*, 69-106. doi: 10.1007/978-3-319-62800-4_2

Eshaghi, A., & Aghaei, A. A. (2015). Effect of TiO_2 graphene nanocomposite photoanode on dye-sensitized solar cell performance. *Bulletin of Materials Science*, *38*(5), 1177-1182. doi: 10.1007/s12034-015-0998-5

Fujisawa, J., Eda, T., & Hanaya, M. (2017). Comparative study of conduction-band and valence-band edges of TiO_2, $SrTiO_3$, and $BaTiO_3$ by ionization potential measurements. *Chemical Physics Letters*, *685*(2017), 23-26. doi: 10.1016/j.cplett.2017.07.031

Gao, F., Wang, Y., Shi, D., Zhang, J., Wang, M., Jing, X., . . . Grätzel, M. (2008). Enhance the optical absorptivity of nanocrystalline TiO_2 film with high molar extinction coefficient ruthenium sensitizers for high performance dye-sensitized solar cells. *Journal of the American Chemical Society*, *130*(32), 10720-10728. doi: 10.1021/ja801942j

Gélinas, S., Rao, A., Kumar, A., Smith, S. L., Chin, A. W., Clark, J., . . . Friend, R. H. (2014). Ultrafast long-range charge separation in organic semiconductor photovoltaic diodes. *Science*, *343*(6170), 512-516. doi: 10.1126/science.1246249

Hanna, R., Nowak, M., Lipinski, L., & Adamowich, L. (1998). Spectral and theoretical investigation on 2- hydroxy- 1,4, naphthoquinone (Lawsone). *Spectrochimica Acta Part A: Molecular Biomolecular Spectroscopy*, *54*, 1091-1103. Retrieved from http://citeseerx.ist.psu.edu/viewdoc/download?doi=10.1.1.735.2774&rep=rep1&type=pdf

Hanwell, M., Curtis, D., Lonie, D., Vandermeersch, T., Zurek, E., & Hutchison, G. (2012). Avogadro: an advanced semantic chemical editor, visualization, and analysis platform. *Journal of Cheminformatics*, *4*(1), doi: 17. 10.1186/1758-2946-4-17

Hao, S., Wu, J., Huang, Y., & Lin, J. (2006). Natural dyes as photosensitizers for dye-sensitized solar cell. *Solar Energy*, *80*(2), 209-214. doi: 10.1016/j.solener.2005.05.009

Hernandez, M., Estevez, M., Vargas, S., Quintanilla, F., & Rodriguez, R. (2011). New dye-sensitized solar cells obtained from extracted bracts of Bougainvillea glabra and spectabilis betalain pigments by different purification processes. *International Journal of Molecular Sciences*, *12*(9), 5565-5576. doi: 10.3390/ijms12095565

Howard, C., Sabine, T., & Dickson, F. (1991). Structural and thermal parameters for rutile and anatase. *Acta Crystallographica Section B: Structural Science*, *47*(4), 462-468. doi: 10.1107/S010876819100335X

Jacquemin, D., Preat, J., Wathelet, V., & Perpète, E. A. (2006). Time-dependent density functional theory determination of the absorption spectra of naphthoquinones. *Chemical Physics*, *328*(1-3), 324-332. doi: 10.1016/j.chemphys.2006.07.037

Jamar, A., Majid, Z., Azmi, W., Norhafana, M., & Razak, A. (2016). A review of water heating system for solar energy applications. *International Communications in Heat Mass Transfer*, *76*, 178-187. doi: 10.1016/j.icheatmasstransfer.2016.05.028

Jeon, J., Park, Y. C., Han, S. S., Goddard III, W. A., Lee, Y. S., & Kim, H. (2014). Rapid dye regeneration mechanism of dye-sensitized solar cells. *The Journal of Physical Chemistry Letters*, *5*(24), 4285-4290. doi: 10.1021/jz502197b

Khadtare, S. S., Ware, A. P., Salunke-Gawali, S., Jadkar, S. R., Pingale, S. S., & Pathan, H. M. (2015). Dye sensitized solar cell with lawsone dye using a ZnO photoanode: experimental and TD-DFT study. *Royal Society of Chemistry Advances*, *5*(23), 17647-17652. doi: 10.1039/C4RA14620D

Kong, L. X., He, M., Yan, W., Zhang, C. S., & Ju, X. H. (2019). Theoretical studies on triaryamine-based p-type D-D-π-A sensitizer. *Journal of the Chinese Chemical Society*, *4*, 1-6. doi: 10.1002/jccs.201800413

Kutraleeswaran, M., Venkatachalam, M., Saroja, M., Gowthaman, P., & Shankar, S. (2017). Dye sensitized solar cells Review. *Journal for Advanced Research in Applied Sciences*, *4*(5), 26-38. doi: 10.1019/ 59df1a22aca27247d7aa2676

Lakshmi, R., Krishnakumar, G., Joseph, L. K., Sreelatha, K., & Jinchu, I. (2016). Lawsone dye complex: an efficient sensitizer for Dye Sensitized Solar Cell: *Paper presented at International Conference on Electrical, Electronics, and Optimization Techniques (ICEEOT)*. (pp. 4636-4638). Chennai, India.

Lee, C., Yang, W., & Parr, R. (1988). Development of the Colle-Salvetti conelation energy formula into a functional of the electron density. *Physical Review Volume B*, *37*, 785-789. Retrieved from https://journals.aps.org/prb/abstract/10.1103/PhysRevB.37.785

Lee, G. H., & Kim, Y. S. (2016). Theoretical study of an asymmetric A-π-D-π-D-π-A′ tribranched organic sensitizer for dye-sensitized solar cells. *Journal of the Korean Physical Society*, *69*(3), 381-385. doi: 10.3938/jkps.69.381

Lemmon, E., McLinden, M., Friend, D., Linstrom, P., & Mallard, W. (2018). NIST Chemistry WebBook, Nist Standard Reference Database Number 69. National Institute of Standards and Technology. Gaithersburg. Retrieved from https://webbook.nist.gov

Li, Y., Jingyan, L., Dixin, L., Xin, L., & Yanling, X. (2019). DA-π-A based organic dyes for efficient DSSCs: A theoretical study on the role of π-spacer. *Computational Materials Science, 161*, 163-176. doi: 10.1016/j.commatsci.2019.01.033

Li, Y., Liu, J., Liu, D., Li, X., & Xu, Y. (2019). DA-π-A based organic dyes for efficient DSSCs: A theoretical study on the role of π-spacer. *Computational Materials Science, 161*, 163-176. doi: 10.1016/j.commatsci.2019.01.033

Lim, A., Kumara, N., Tan, A., Mirza, A., Chandrakanthi, R., & Petra, M. (2015). Potential natural sensitizers extracted from the skin of Canarium odontophyllum fruits for dye-sensitized solar cells. *Spectrochimica Acta Part A: Molecular and Biomolecular Spectroscopy*, *138*, 596-602. doi: 10.1016/j.saa.2014.11.102

Liu, Q., Ren, P., Wang, X., Li, Y., & Yang, Y. (2018). Experimental and Theoretical Investigation of the Photoelectrical Properties of Tetrabromophenol Blue-and Bromoxylenol Blue-Based Solar Cells. *Journal of Nanomaterials, 2018*, 1-14. doi: 10.1155/2018/9720595

Ludin, N. A., Mahmoud, A. A.-A., Mohamad, A. B., Kadhum, A. A. H., Sopian, K., & Karim, N. S. A. (2014). Review on the development of natural dye photosensitizer for dye-sensitized solar cells. *Renewable Sustainable Energy Reviews, 31*, 386-396. doi: 10.1016/j.rser.2013.12.001

Lyons, C., Dev, P., Maji, P., Rathi, N., Surolia, P. K., Byrne, O., . . . MacElroy, J. (2018). Silicon-bridged triphenylamine-based organic dyes for efficient dye-sensitised solar cells. *Solar Energy, 160*, 64-75. doi: 10.1016/j.solener.2017.11.070

Madili, N., Pogrebnoi, A., & Pogrebnaya, T. (2018). Theoretical Design of Complex Molecule via Combination of Natural Lawsone and Synthetic Indoline D131 Dyes for Dye Sensitized Solar Cells Application. *Computational Chemistry, 6*(1), 87-112. doi: 10.4236/cc.2018.64007

Mahkam, M., Kafshboran, H., & Nabati, M. (2014). Synthesis and characterization of novel colored polymers based on lawsone natural compound. *Designed Monomers and Polymers*, *17*(8), 784-794. doi: 10.1080/15685551.2014.918017

Mathew, S., Yella, A., Gao, P., Humphry-Baker, R., Curchod, B. F., Ashari-Astani, N., . . . Grätzel, M. (2014). Dye-sensitized solar cells with 13% efficiency achieved through the molecular engineering of porphyrin sensitizers. *Nature Chemistry*, *6*(3), 242. doi: 10.1038/nchem.1861

Millefiori, S., Gulino, A., & Casarin, M. (1990). UV photoelectron spectra, reduction potentials and MO calculations of intramolecularly hydrogen-bonded naphthoquinones. *Journal de Chimie Physique*, *87*, 317-330. doi: 10.1051/jcp/1990870317

Msangi, A., Pogrebnoi, A., & Pogrebnaya, T. (2018). Combination of Natural Dye (Crocetin) and Synthetic Dye (Indoline D205) for DSSCs Application. *International Journal of Computational and Theoretical Chemistry.*, *6*, 1-13. doi: 10.11648/j.ijctc.20180601.11

Nazeeruddin, M. K., Baranoff, E., & Grätzel, M. (2011). Dye-sensitized solar cells: a brief overview. *Solar Energy*, *85*(6), 1172-1178. doi: 10.1016/j.solener.2011.01.018

Nazeeruddin, M. K., Pechy, P., Renouard, T., Zakeeruddin, S. M., Humphry-Baker, R., Comte, P., . . . Shklover, V. (2001). Engineering of efficient panchromatic sensitizers for nanocrystalline TiO_2 based solar cells. *Journal of the American Chemical Society*, *123*(8), 1613-1624. doi: 10.1021/ja003299u

Nguyen, L. H., Mulmudi, H. K., Sabba, D., Kulkarni, S. A., Batabyal, S. K., Nonomura, K., . . . Mhaisalkar, S. G. (2012). A selective co-sensitization approach to increase photon conversion efficiency and electron lifetime in dye-sensitized solar cells. *Physical Chemistry Chemical Physics*, *14*(47), 16182-16186. doi: 10.1039/C2CP42959D

O'Regan, B., & Grätzel, M. (1991). A low-cost, high-efficiency solar cell based on dye-sensitized colloidal TiO_2 films. *Nature*, *353*(6346), 737. doi: 10.1038/353737a0

Oda, Y., Nakashima, S., Kondo, E., Nakamura, S., Yano, M., Kubota, C., . . . Matsuda, H. (2018). Comparison of lawsone contents among Lawsonia inermis plant parts and neurite outgrowth accelerators from branches. *Journal of Natural Medicines*, *72*(4), 890-896. doi: 10.1007/s11418-018-1221-y

Ogura, R. Y., Nakane, S., Morooka, M., Orihashi, M., Suzuki, Y., & Noda, K. (2009). High-performance dye-sensitized solar cell with a multiple dye system. *Applied Physics Letters*, *94*(7), 54. doi: 10.1063/1.3086891

Oprea, C. I., Frecuş, B., Minaev, B. F., & Gîrţu, M. A. (2011). DFT study of electronic structure and optical properties of some Ru-and Rh-based complexes for dye-sensitized solar cells. *Molecular Physics*, *109*(21), 2511-2523. doi: 10.1080/00268976.2011.621454

Pavia, D. L., Lampman, G. M., & Kriz, G. S.(2001). 3. *Introduction to Spectroscopy*. Western Washington University. CA: Bellingham, Washington.

Pawar, A. B., Jadhav, K. D., Wadekar, M. P., & Sarawadekar, R. G. (2011). Spectral and theoretical investigation on 2-hydroxy-1, 4-naphthoquinone (lawsone). *Journal of Pharmacy Research*, *4*(6), 1745-1747. doi: 10.1.1.735.2774

Preat, J., Jacquemin, D., & Perpète, E. A. (2010). Design of new triphenylamine-sensitized solar cells: a theoretical approach. *Environmental Science and Technology*, *44*(14), 5666-5671. doi: 10.1021/es100920j

Rani, S., Shishodia, P., & Mehra, R. (2010). Development of a dye with broadband absorbance in visible spectrum for an efficient dye-sensitized solar cell. *Journal of Renewable Sustainable Energy*, *2*(4), 043103. doi: 10.1063/1.3463056

Reshak, A. H., Shahimin, M., Juhari, N., & Vairavan, R. (2013). Photovoltaic characteristics of hybrid MEH-PPV-nanoparticles compound. *Current Applied Physics*, *13*(9), 1894-1898. doi: 10.1016/j.cap.2013.07.023

Schmidt, M. W., Baldridge, K. K., Boatz, J. A., Elbert, S. T., Gordon, M. S., Jensen, J. H., . . . Su, S. (1993). General atomic and molecular electronic structure system. *Journal of Computational Chemistry*, *14*(11), 1347-1363. doi: 10.1002/jcc.540141112

Shalini, S., Balasundaraprabhu, R., Kumar, T. S., Prabavathy, N., Senthilarasu, S., & Prasanna, S. (2016). Status and outlook of sensitizers/dyes used in dye sensitized solar cells (DSSC): a review. *International Journal of Energy Research*, *40*(10), 1303-1320. doi: 10.1002/er.3538

Shelke, R., Thombre, S., & Patrikar, S. (2017). Status and perspectives of dyes used in dye sensitized solar cells. *International Journal of Renewable Energy Resources*, *3*(2), 54-61. Retrieved from http://www.8026-1237-16860-1-10-20171017%20(7).pdf

Shinde, D., Tambade, P., Gadave, K., Pawar, K., Naushad, M., & Pathan, H. (2017). Dye-sensitized solar cells with a naturally occurring pigment lycopene as a photosensitizer for zirconium dioxide: an experimental and theoretical study. *Journal of Materials Science: Materials in Electronics*, *28*(15), 11311-11316. doi: 10.1007/s10854-017-6923-5

Sinopoli, A., Citro, I., Calogero, G., & Bartolotta, A. (2017). Combined experimental and DFT-TDDFT investigation on anthocyanidins for application in dye-sensitised solar cells. *Dyes Pigments*, *143*, 291-300. doi: 10.1016/j.dyepig.2017.04.018

Smestad, G. P., & Gratzel, M. (1998). Demonstrating electron transfer and nanotechnology: a natural dye-sensitized nanocrystalline energy converter. *Journal of Chemical Education*, *75*(6), 752. doi: 10.1021/ed075p752

Song, W., Gong, Y., Tian, J., Cao, G., Zhao, H., & Sun, C. (2016). Novel photoanode for dye-sensitized solar cells with enhanced light-harvesting and electron-collection efficiency. *America Chemistry of Society Applied Materials Interfaces*, *8*(21), 13418-13425. doi: 10.1021/acsami.6b02887

Suhaimi, S., Shahimin, M. M., Alahmed, Z., Chyský, J., & Reshak, A. (2015). Materials for enhanced dye-sensitized solar cell performance: Electrochemical application. *International Journal of Electrochemical Science*, *10*(4), 2859-2871. doi: 10.1036/54f3d8860cf2f9e34f084c14

Sun, C., Li, Y., Song, P., & Ma, F. (2016). An experimental and theoretical investigation of the electronic structures and photoelectrical properties of ethyl red and carminic acid for DSSC application. *Materials, 9*(10), 813. doi: 10.3390/ma9100813

Syafinar, R., Gomesh, N., Irwanto, M., Fareq, M., & Irwan, Y. (2015). Chlorophyll pigments as a nature-based dye for dye-sensitized solar cell (DSSC). *Energy Procedia*, *79*, 896-902. doi: 10.1016/j.egypro.2015.11.584

Tanaka, K., Tamamushi, R., & Ogawa, T. (1985). Bioelectrochemical fuel cell operated by the cyanobacterium, Anabaena variabilis. *Journal of Chemical Technology Biotechnology*, *35*(3), 191-197. doi: 10.1002/jctb.280350304

Todkary, A. V., Dalvi, R., Salunke-Gawali, S., Linares, J., Varret, F., Marrot, J., . . . Gejji, S. P. (2006). SOM assembly of hydroxynaphthoquinone and its oxime: Polymorphic X-ray structures and EPR studies. *Spectrochimica Acta Part A: Molecular Biomolecular Spectroscopy*, *63*(1), 130-138. doi: 10.1016/j.saa.2005.04.054

Vessecchi, R., Emery, F. S., Galembeck, S. E., & Lopes, N. P. (2012). Gas-phase reactivity of 2-hydroxy-1, 4-naphthoquinones: a computational and mass spectrometry study of lapachol congeners. *Journal of Mass Spectrometry*, *47*(12), 1648-1659. doi: 10.1002/jms.3101

Vosko, S. H., Wilk, L., & Nusair, M. (1980). Accurate spin-dependent electron liquid correlation energies for local spin density calculations: a critical analysis. *Canadian Journal of Physics*, *58*(8), 1200-1211. doi: 10.1139/p80-159

Wang, X., Fan, R., Dong, Y., Su, T., Huang, J., Du, X., . . . Yang, Y. (2017). Metal (II)-induced synthesis of asymmetric fluorescence benzimidazoles complexes and their dye-sensitized solar cell performance as cosensitizers. *Crystal Growth Design*, *17*(10), 5406-5421. doi: 10.1021/acs.cgd.7b00891

Wei, L., Wang, P., Yang, Y., Fan, R., Yang, Y., & Qiu, Y. (2017). Construction of efficient photoanodes for dye sensitized solar cells: TiO_2 films with a gradient content of graphene. *Sustainable Energy Fuels*, *1*(5), 1112-1122. doi: 10.1039/C7SE00192D

Yamazaki, E., Murayama, M., Nishikawa, N., Hashimoto, N., Shoyama, M., & Kurita, O. (2007). Utilization of natural carotenoids as photosensitizers for dye-sensitized solar cells. *Solar Energy*, *81*(4), 512-516. doi: 10.1016/j.solener.2006.08.003

Zanjanchi, F., & Beheshtian, J. (2019). Natural pigments in dye-sensitized solar cell (DSSC): a DFT-TDDFT study. *Journal of the Iranian Chemical Society*, *16*(4), 795-805. doi: 10.1007/s13738-018-1561-2

Zaware, S. B., Gonnade, R. G., Srinivas, D., Khan, A., & Rane, S. Y. (2011). Antioxidant and anticancer activities of supramolecularly controlled magnetostructural halo-oximes of lawsone. *New Journal of Chemistry*, *35*(8), 1615-1623. doi: 10.1039/C1NJ20176J

Zhang, G., Bai, Y., Li, R., Shi, D., Wenger, S., Zakeeruddin, S. M., . . . Wang, P. (2009). Employ a bisthienothiophene linker to construct an organic chromophore for efficient and stable dye-sensitized solar cells. *Energy Environmental Science*, *2*(1), 92-95. doi: 10.1039/B817990E

Zhang, G., & Musgrave, C. B. (2007). Comparison of DFT methods for molecular orbital eigenvalue calculations. *The Journal of Physical Chemistry A*, *111*(8), 1554-1561. doi: 10.1021/jp061633o

Zhao, D., Lu, Q., Su, R., Li, Y., & Zhao, M. (2019). Light Harvesting and Optical-Electronic Properties of Two Quercitin and Rutin Natural Dyes. *Applied Sciences*, *9*(12), 2567. doi: 10.3390/app9122567

Zhou, H., Wu, L., Gao, Y., & Ma, T. (2011). Dye-sensitized solar cells using 20 natural dyes as sensitizers. *Journal of Photochemistry and Photobiology A: Chemistry*, *219*(2-3), 188-194. doi: 10.1016/j.jphotochem.2011.02.008

Zhurko, A. G., & Zhurko, D. A. (2015). Chemcraft Graphical Program for Visualization of Computed Results. Retrieved from http://www.chemcraftprog.com/

APPENDIX

The thermodynamic functions for two isomers of lawsone (L′ and L), lawsone ether (LE) and bilawsone (BL) are listed in Table A. The values of molar heat capacity (C_p^o), entropy $S°(T)$ and reduced Gibbs free energy $\Phi°(T)$ are given in J mol^{-1} K^{-1} and enthalpy increments $H°(T)–H°(0)$ is given in kJ mol^{-1}.

Table A: Thermodynamic functions of lawsone isomers (L′ and L), LE and BL.

T, K	C_p^o	$S°(T)$	$H°(T)–H°(0)$	$\Phi°(T)$
Lawsone L′				
298.15	169.1	405.1	27.9	311.4
300	170.1	406.2	28.3	312.0
350	194.6	434.3	37.4	327.5
400	217.2	461.8	47.7	342.6
450	237.8	488.6	59.1	357.3
500	256.2	514.6	71.4	371.7
550	272.7	539.8	84.7	385.9
600	287.3	564.2	98.7	399.7
Lawsone L				
298.15	166.5	400.7	27.4	308.8
300	167.5	401.8	27.7	309.4
350	192.2	429.5	36.7	324.6
400	215.1	456.6	46.9	339.4
450	235.8	483.2	58.2	353.9
500	254.5	509.0	70.4	368.1
550	271.1	534.1	83.6	382.1
600	285.9	558.3	97.5	395.8
LE				
298.15	317.7	609.9	52.2	434.9
300	319.6	612.1	52.8	436.1
350	366.2	664.9	69.9	465.0
400	409.4	716.6	89.4	493.2
450	448.6	767.1	110.8	520.9
500	483.9	816.3	134.2	548.0
550	515.3	863.9	159.1	574.5
600	543.3	909.9	185.6	600.6
BL				
298.15	332.4	607.8	54.0	426.5
300	334.3	609.9	54.6	427.8
350	382.1	665.1	72.6	457.7
400	426.3	719.0	92.8	487.0
450	466.3	771.6	115.1	515.7
500	502.2	822.6	139.4	543.9
550	534.2	872.0	165.3	571.5
600	562.7	919.7	192.7	598.5